Supplementary Information

Effect of bridgehead substitution in the Grob fragmentation of norbornyl ketones: A new route to substituted halophenols

Sumit Choudhury,[§] Saeed Ahmad,[§] and Faiz Ahmed Khan[*†]

[§]Department of Chemistry, Indian Institute of Technology Kanpur-208016, India

[†]Department of Chemistry, Indian Institute of Technology Hyderabad, Ordnance Factory Estate, Yeddumailaram-502205, India

E-mail: faiz@iith.ac.in

Table of Contents

1. ^{1}H and ^{13}C NMR spectra of compounds

^{1}H NMR (400 MHz) and ^{13}C NMR (100 MHz) of **12a-13a**

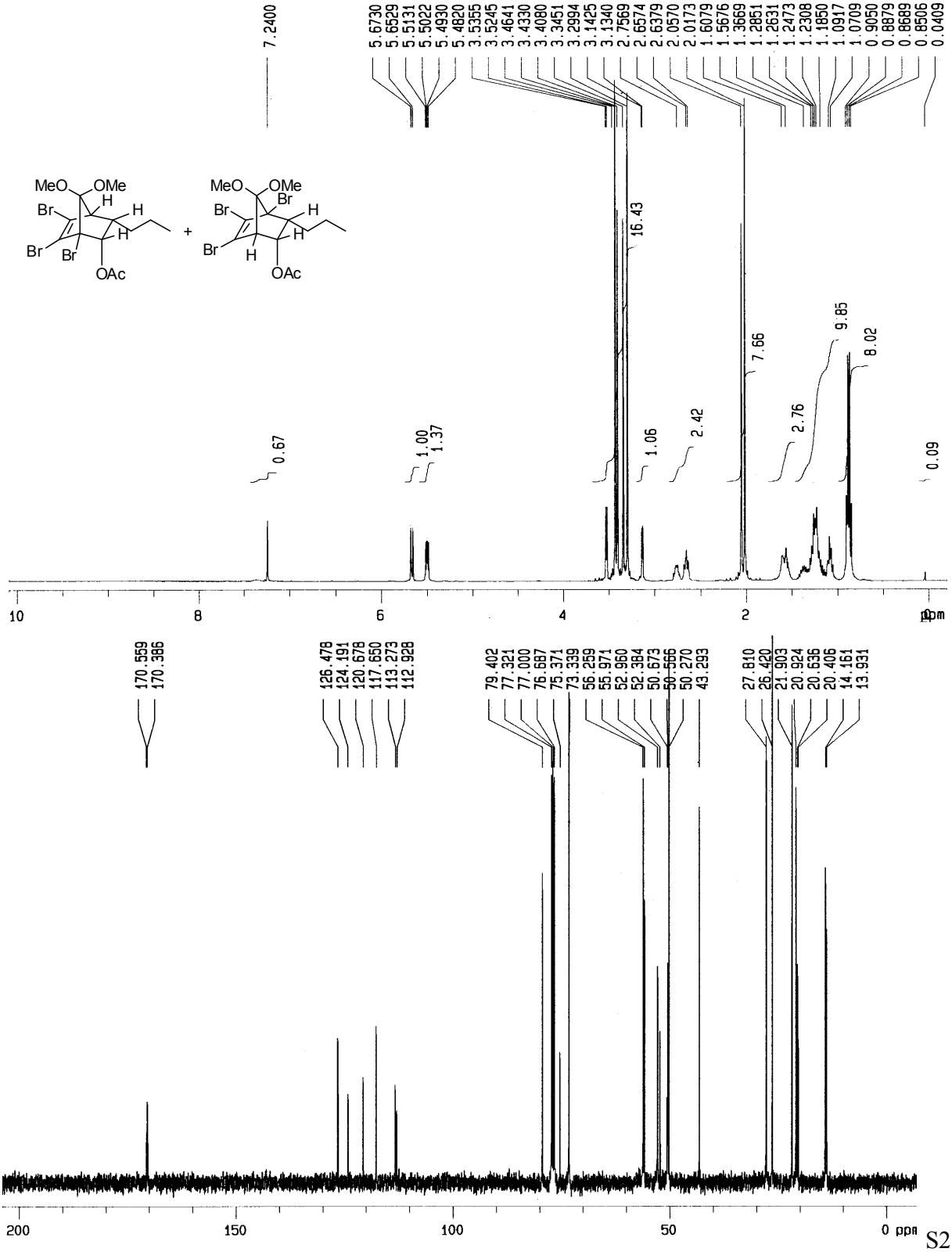

^{1}H NMR (400 MHz) and ^{13}C NMR (100 MHz) of **12b-13b**

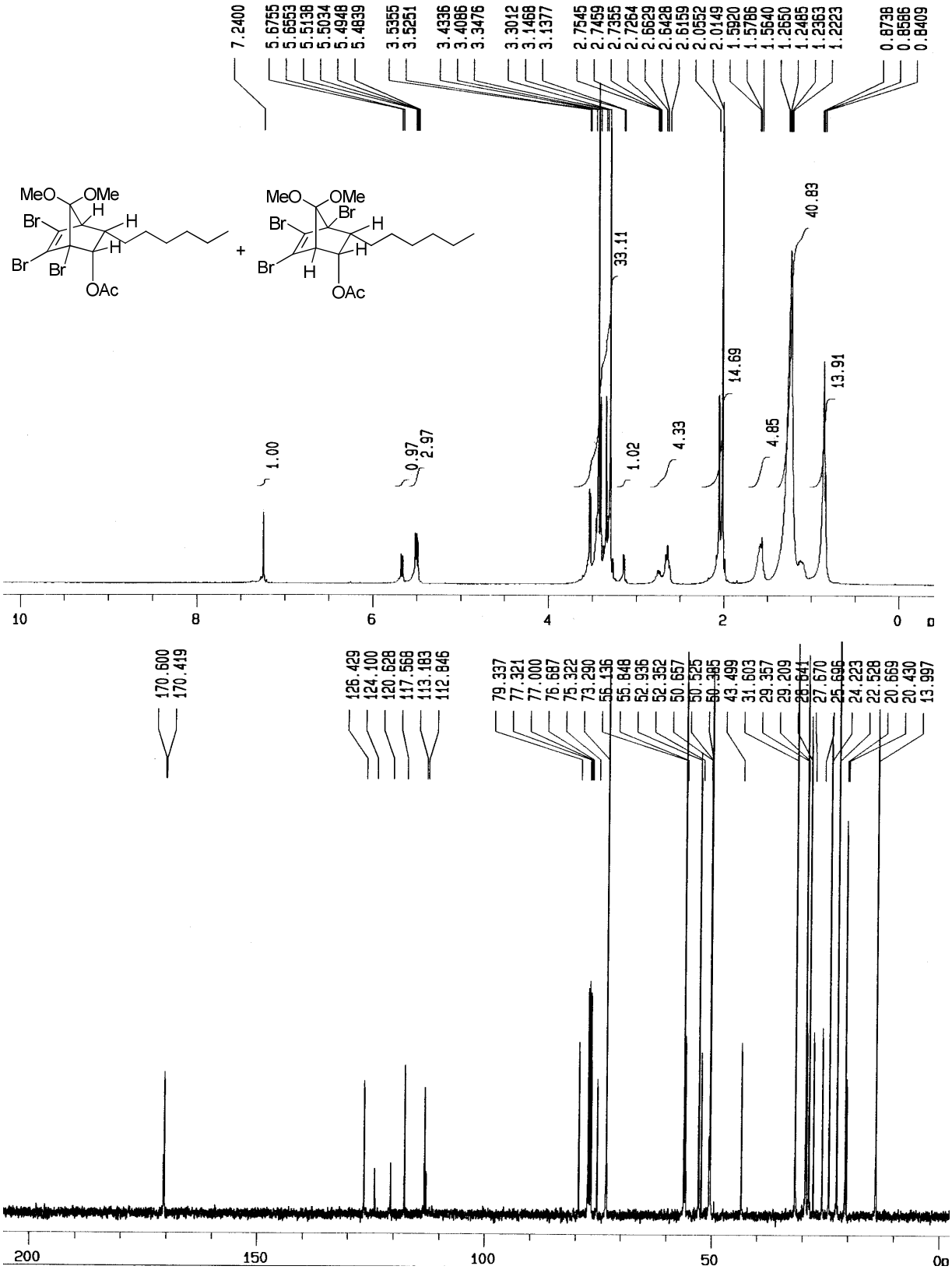

^{1}H NMR (400 MHz) and ^{13}C NMR (100 MHz) of **12c-13c**

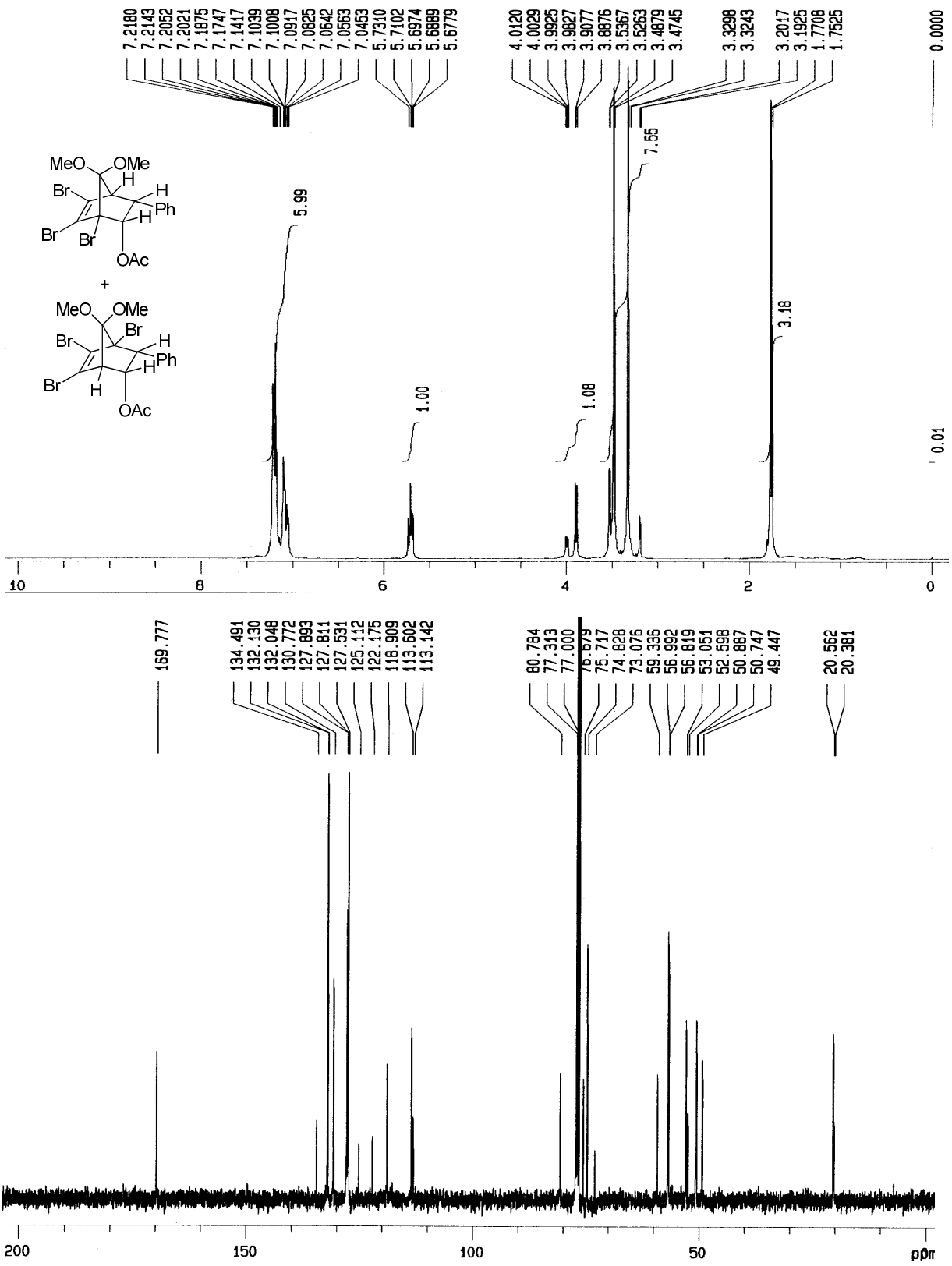

^{1}H NMR (400 MHz) and ^{13}C NMR (100 MHz) of **12d-13d**

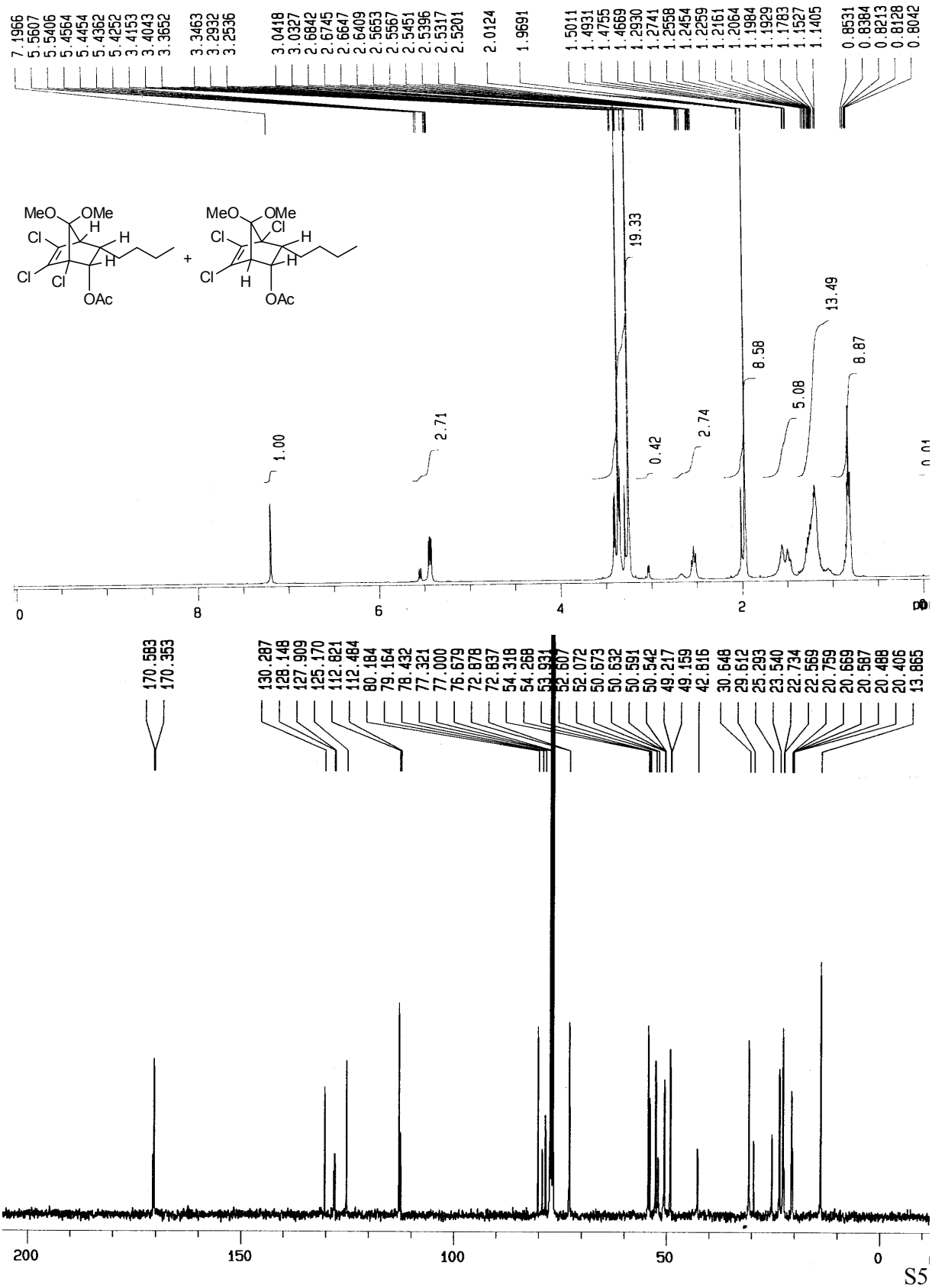

^{1}H NMR (400 MHz) and ^{13}C NMR (100 MHz) of **15a**

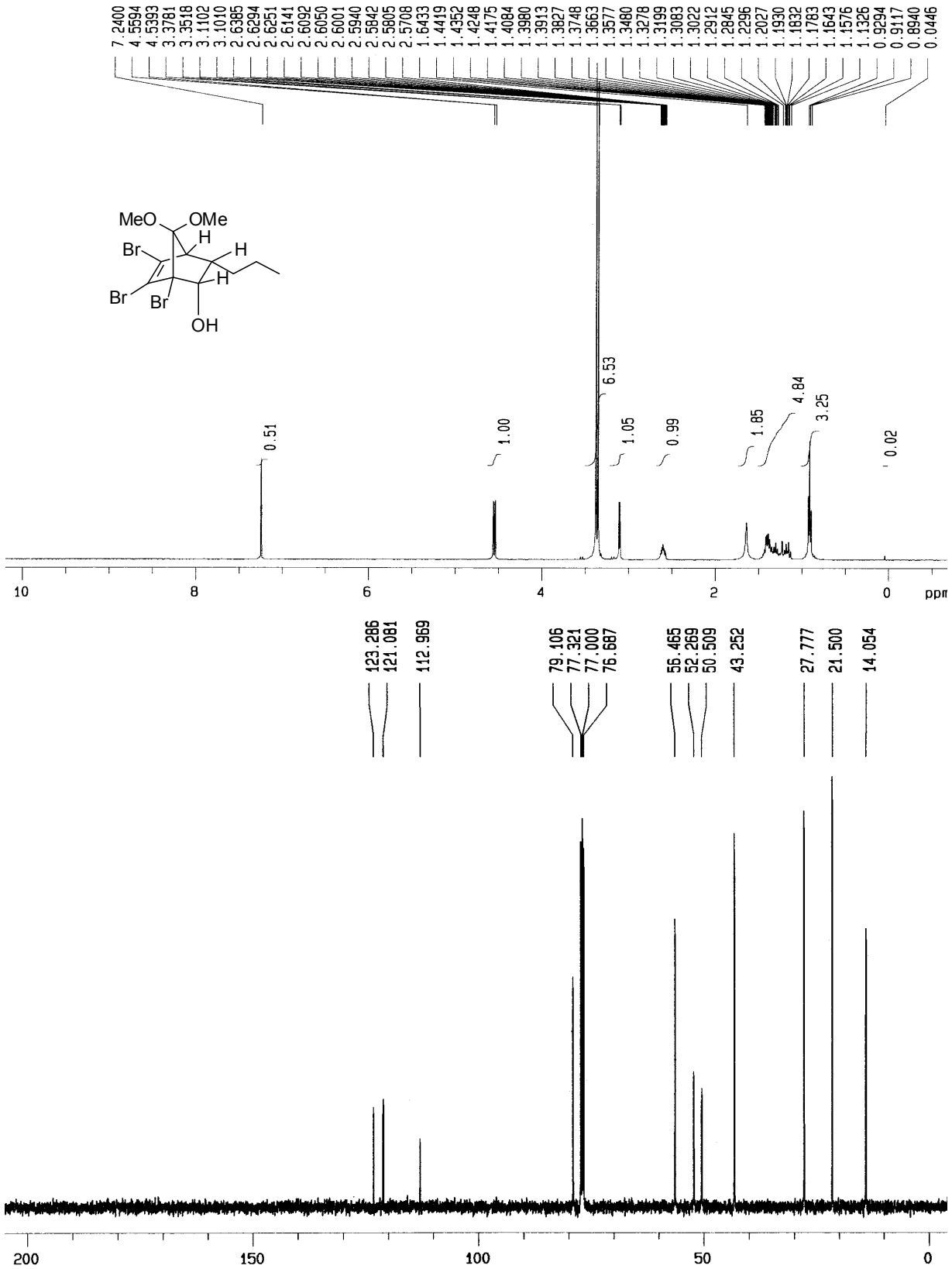

^{1}H NMR (400 MHz) and ^{13}C NMR (100 MHz) of **16a**

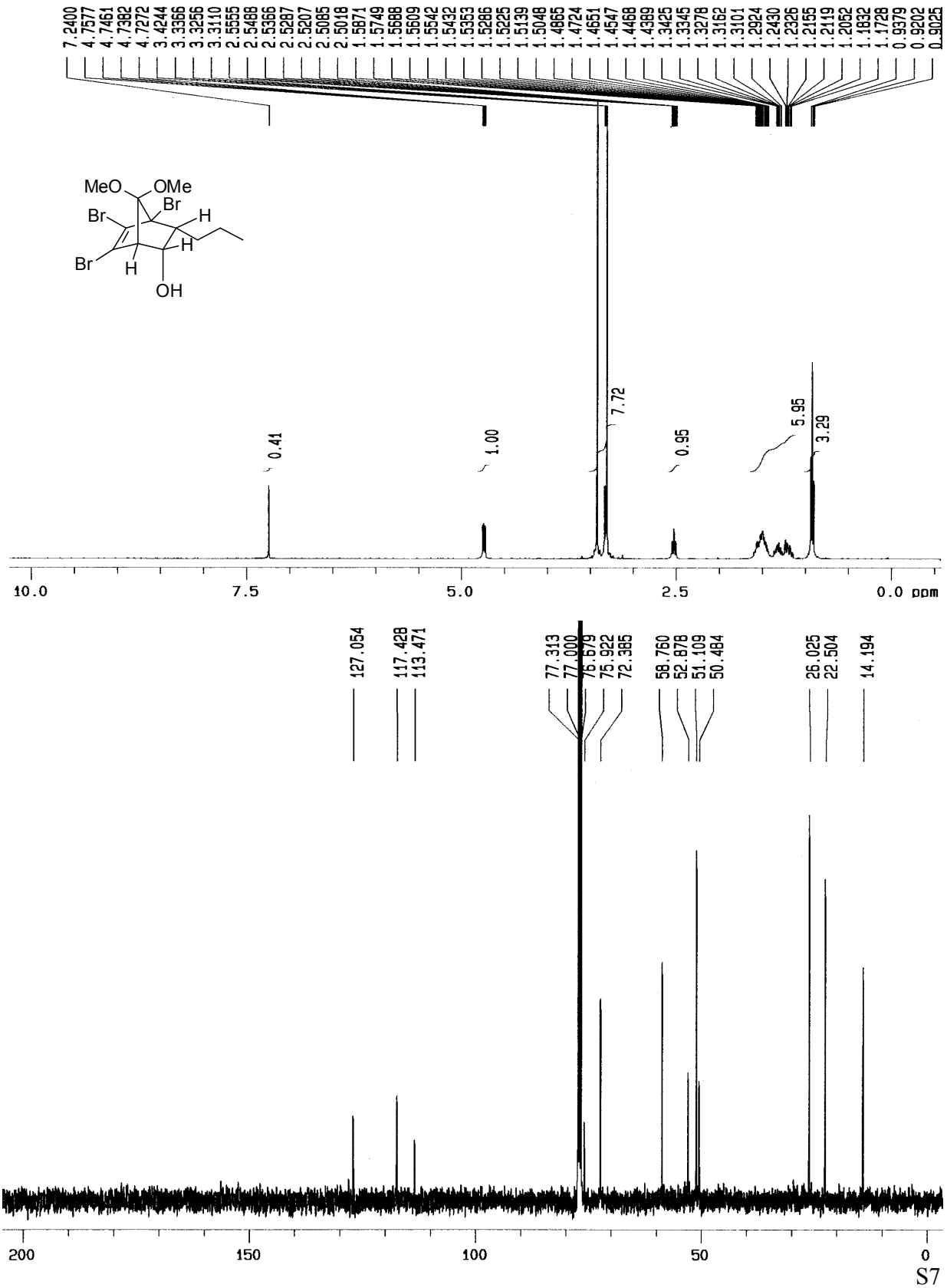

^{1}H NMR (400 MHz) and ^{13}C NMR (100 MHz) of **15b**

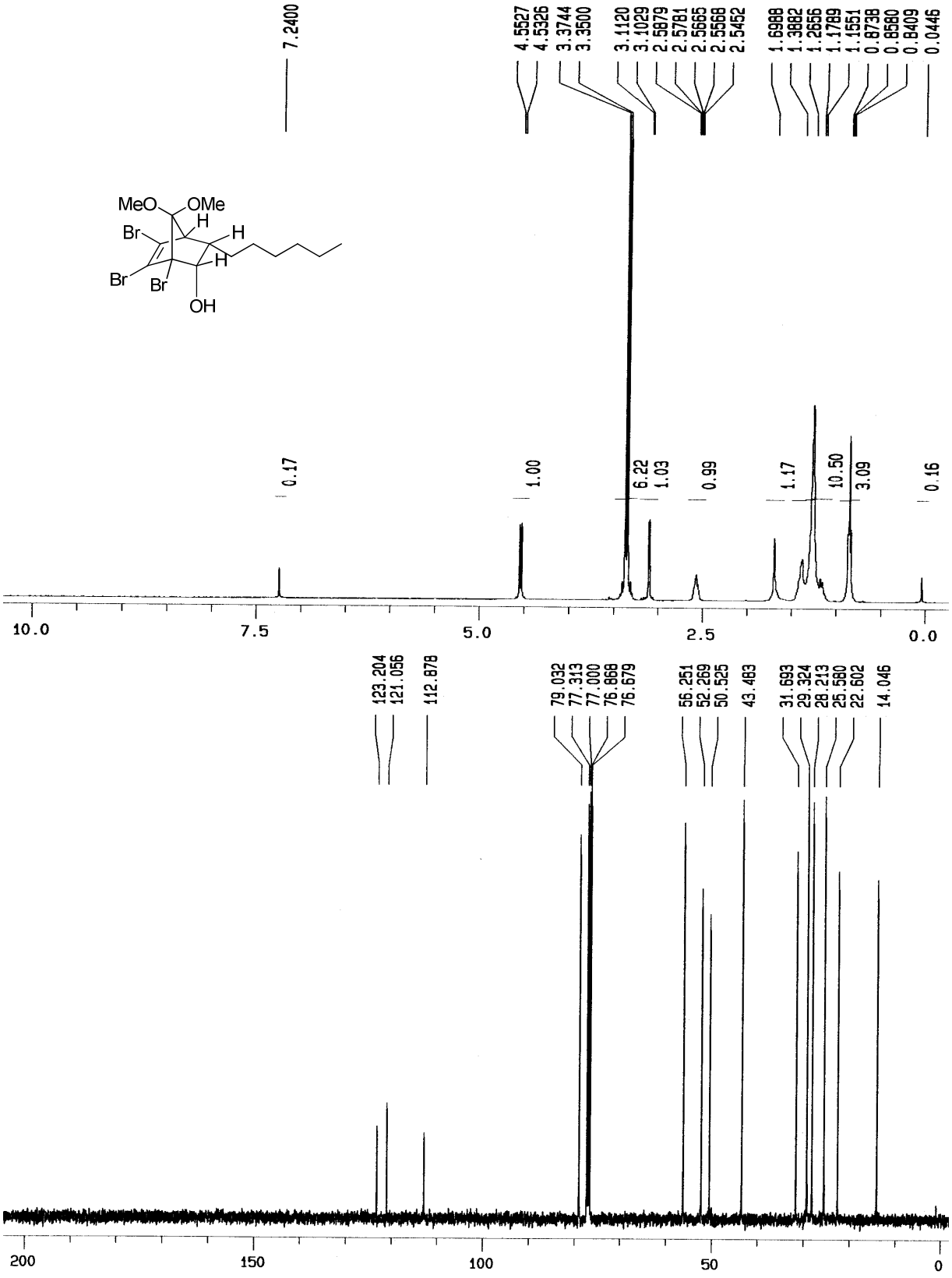

^{1}H NMR (400 MHz) and ^{13}C NMR (100 MHz) of **16b**

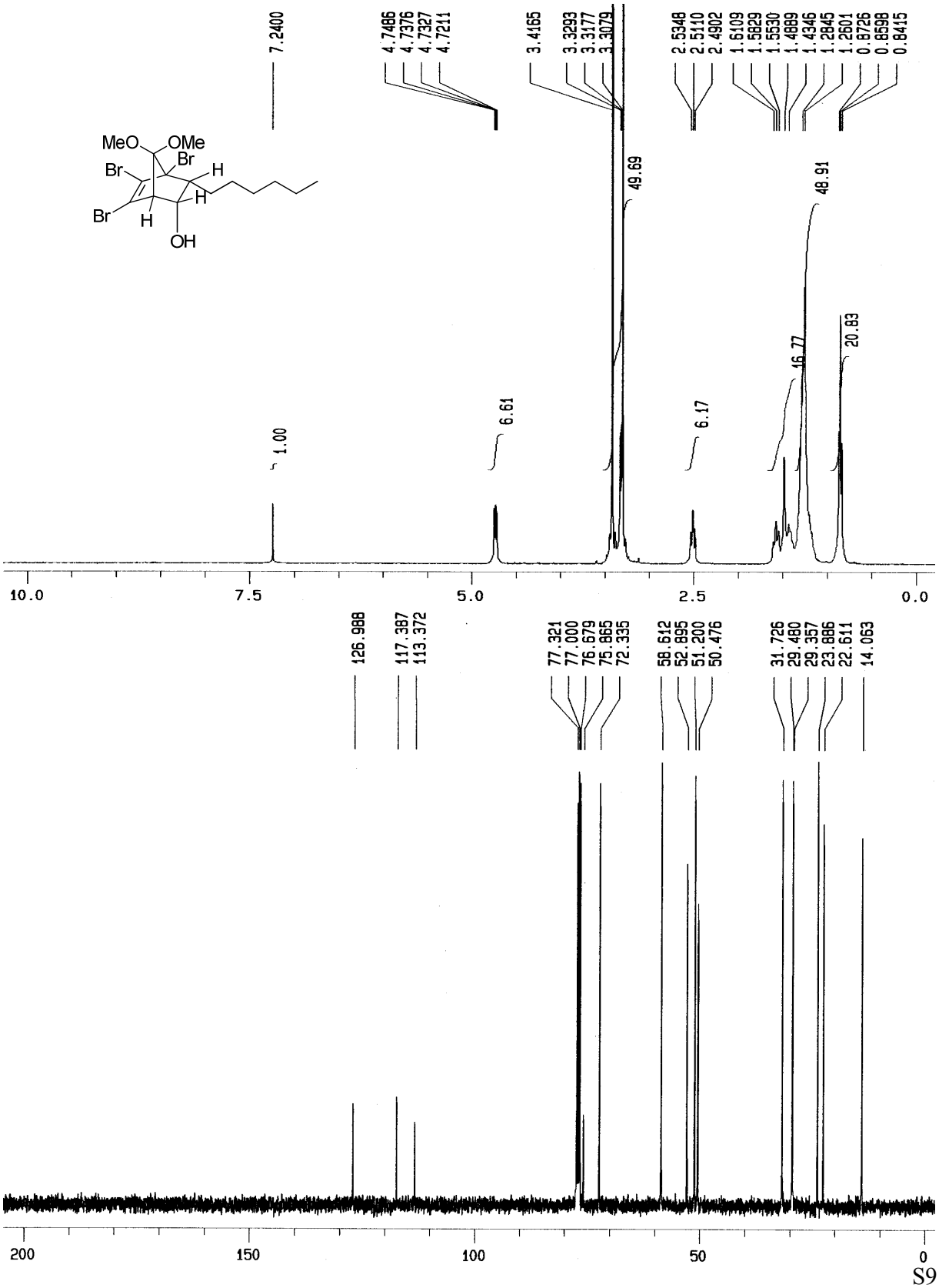

^{1}H NMR (400 MHz) and ^{13}C NMR (100 MHz) of **15c**

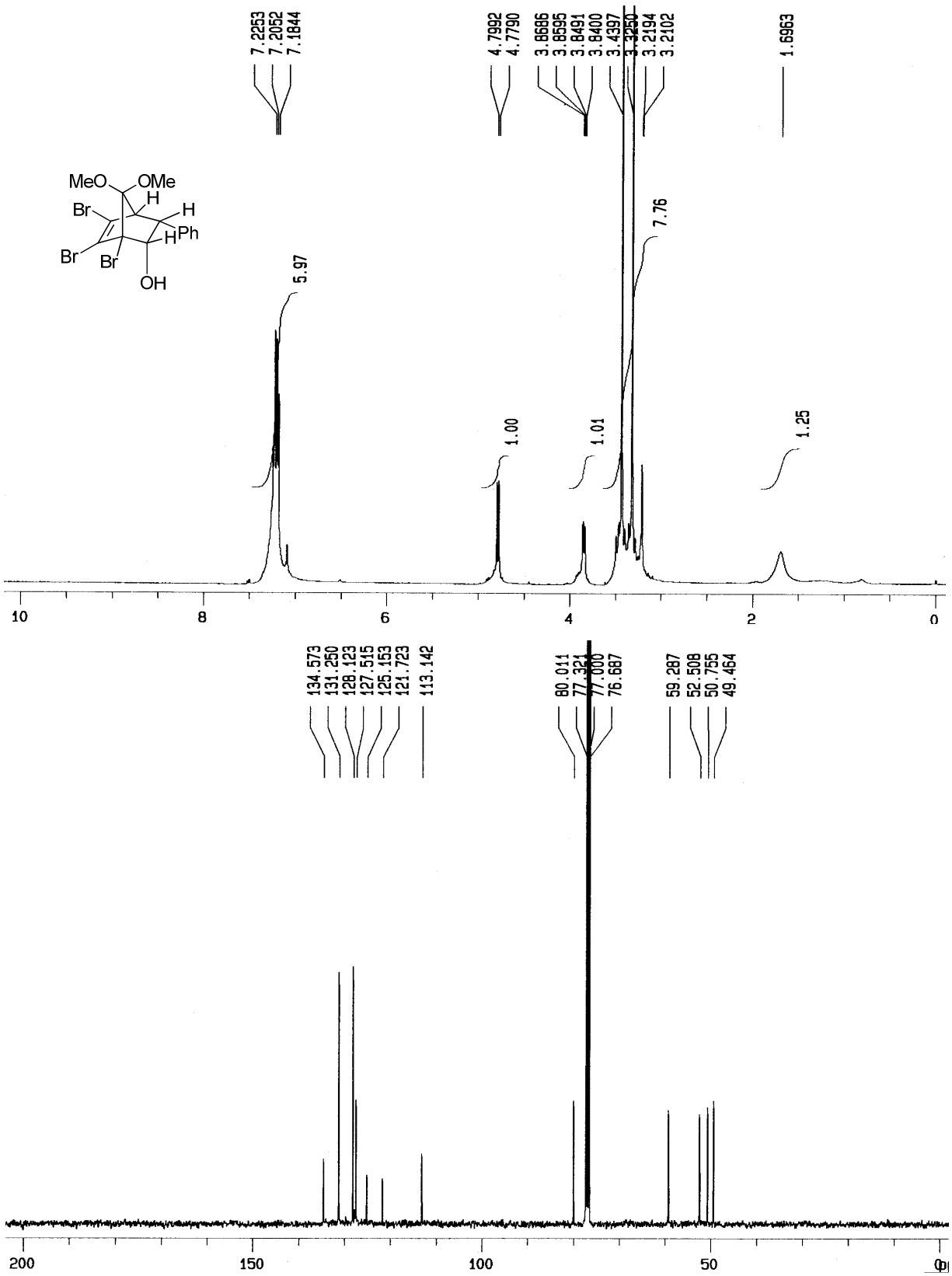

^{1}H NMR (400 MHz) and ^{13}C NMR (100 MHz) of **16c**

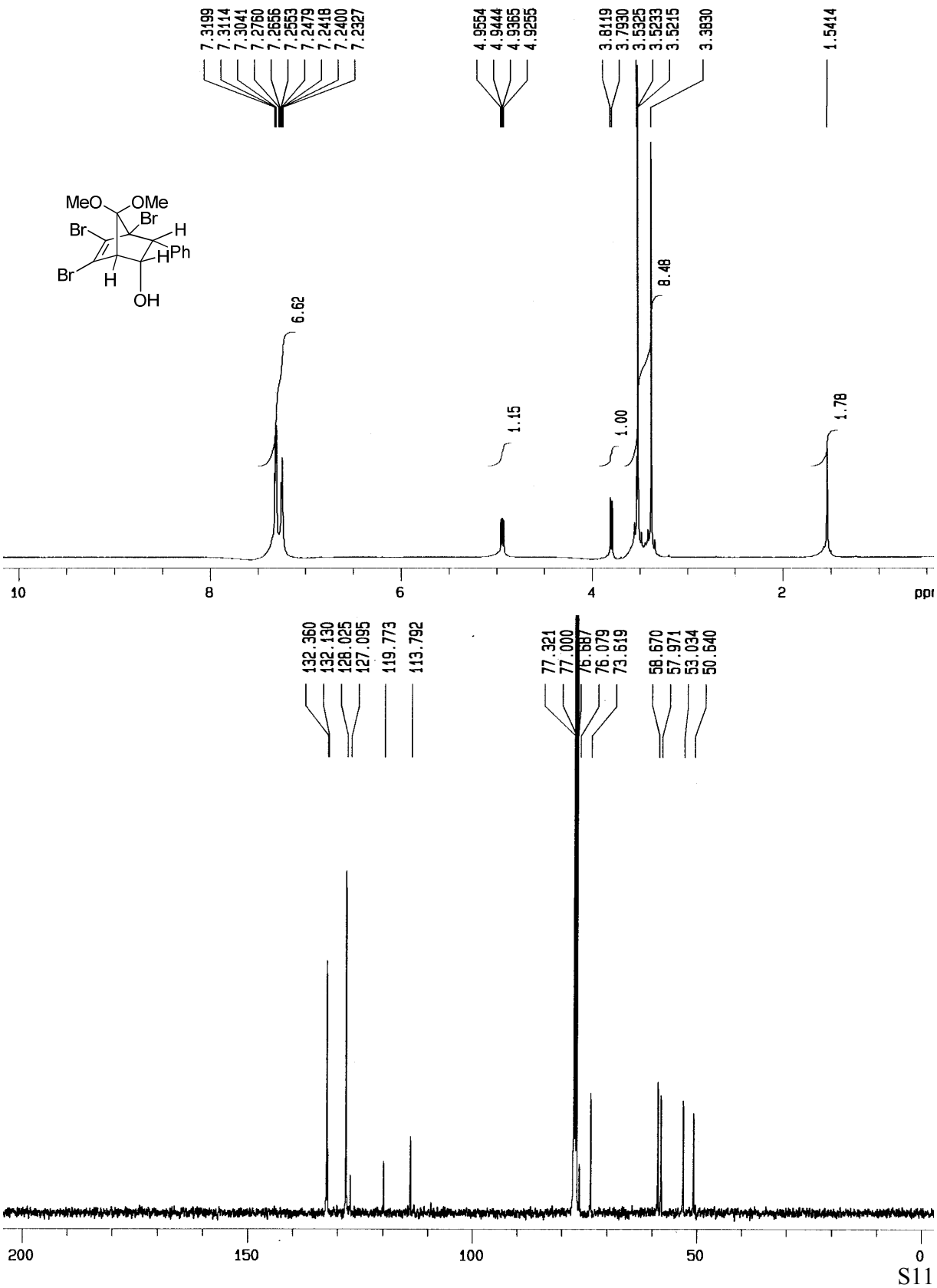

^{1}H NMR (400 MHz) and ^{13}C NMR (100 MHz) of **15d**

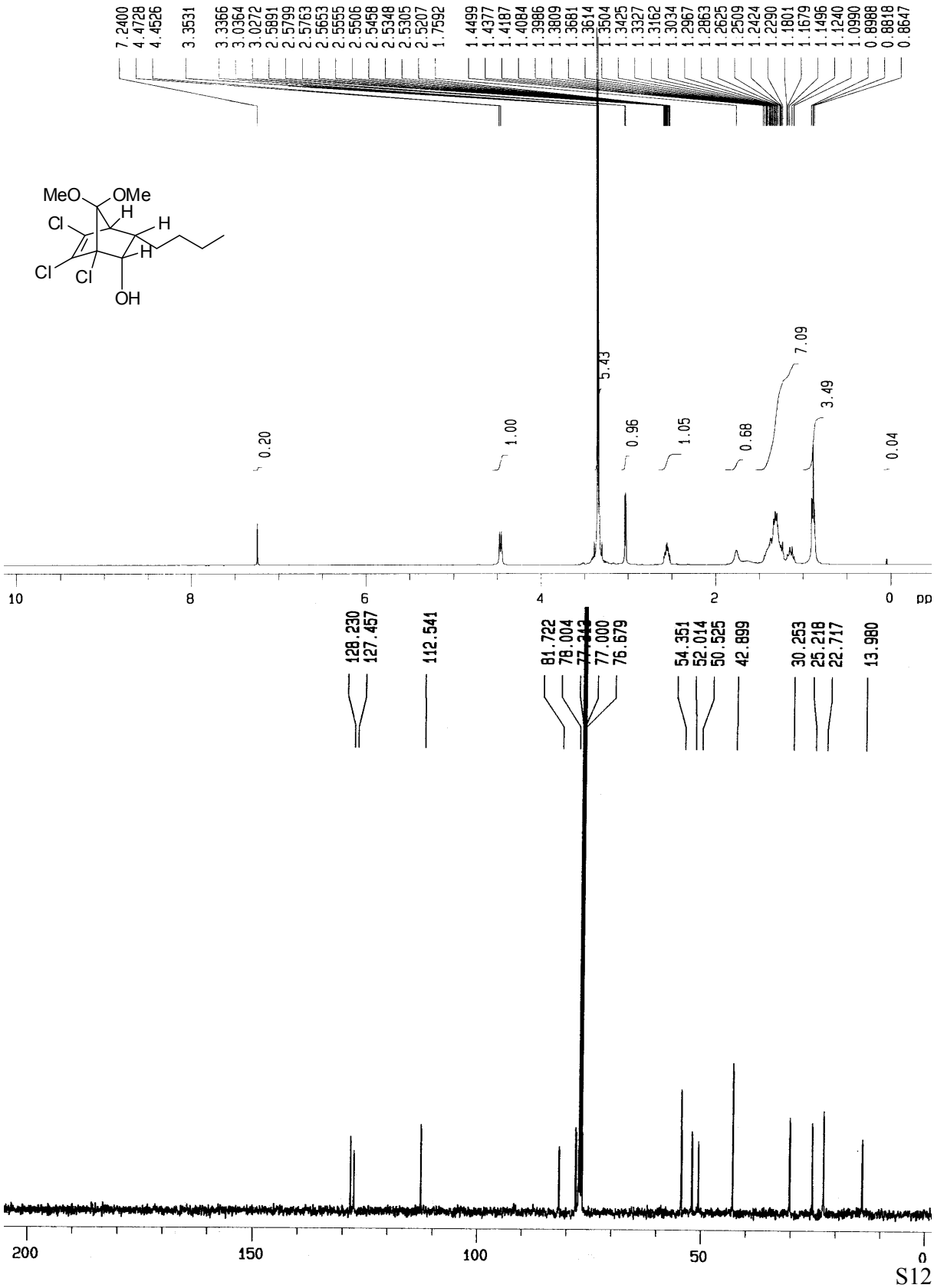

^{1}H NMR (400 MHz) and ^{13}C NMR (100 MHz) of **16d**

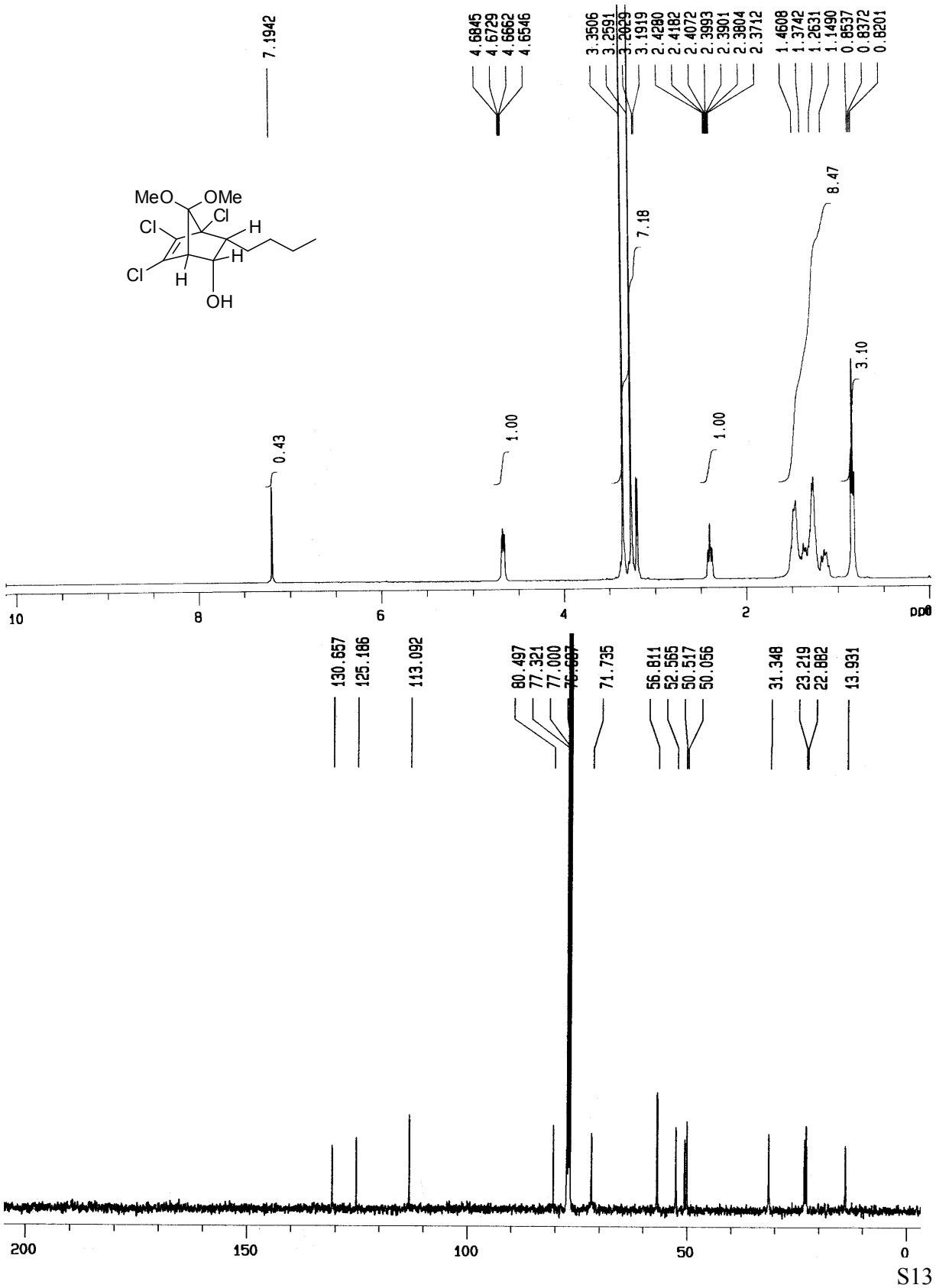

^{1}H NMR (400 MHz) and ^{13}C NMR (100 MHz) of **9a**

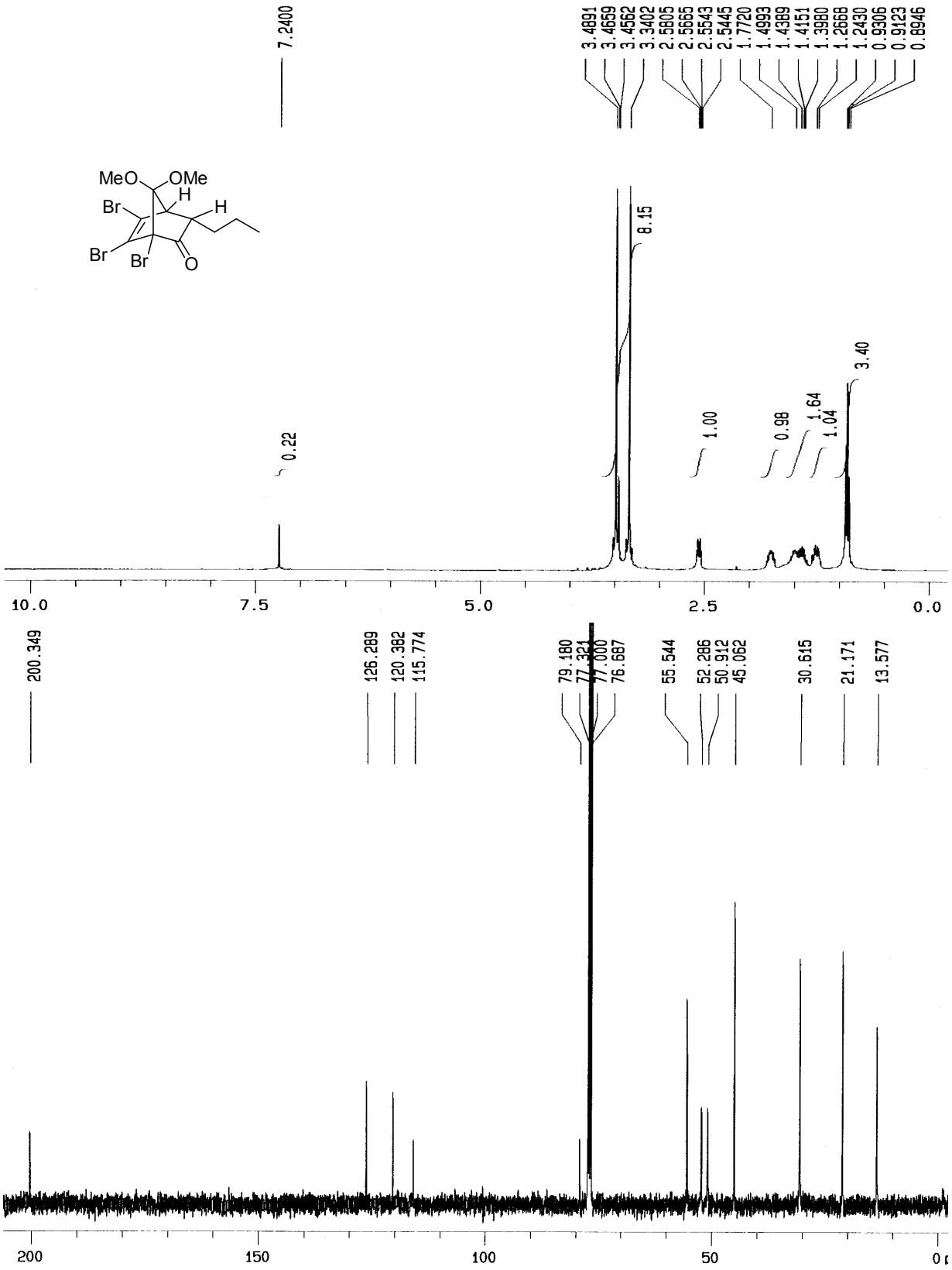

^{1}H NMR (400 MHz) and ^{13}C NMR (100 MHz) of **10a**

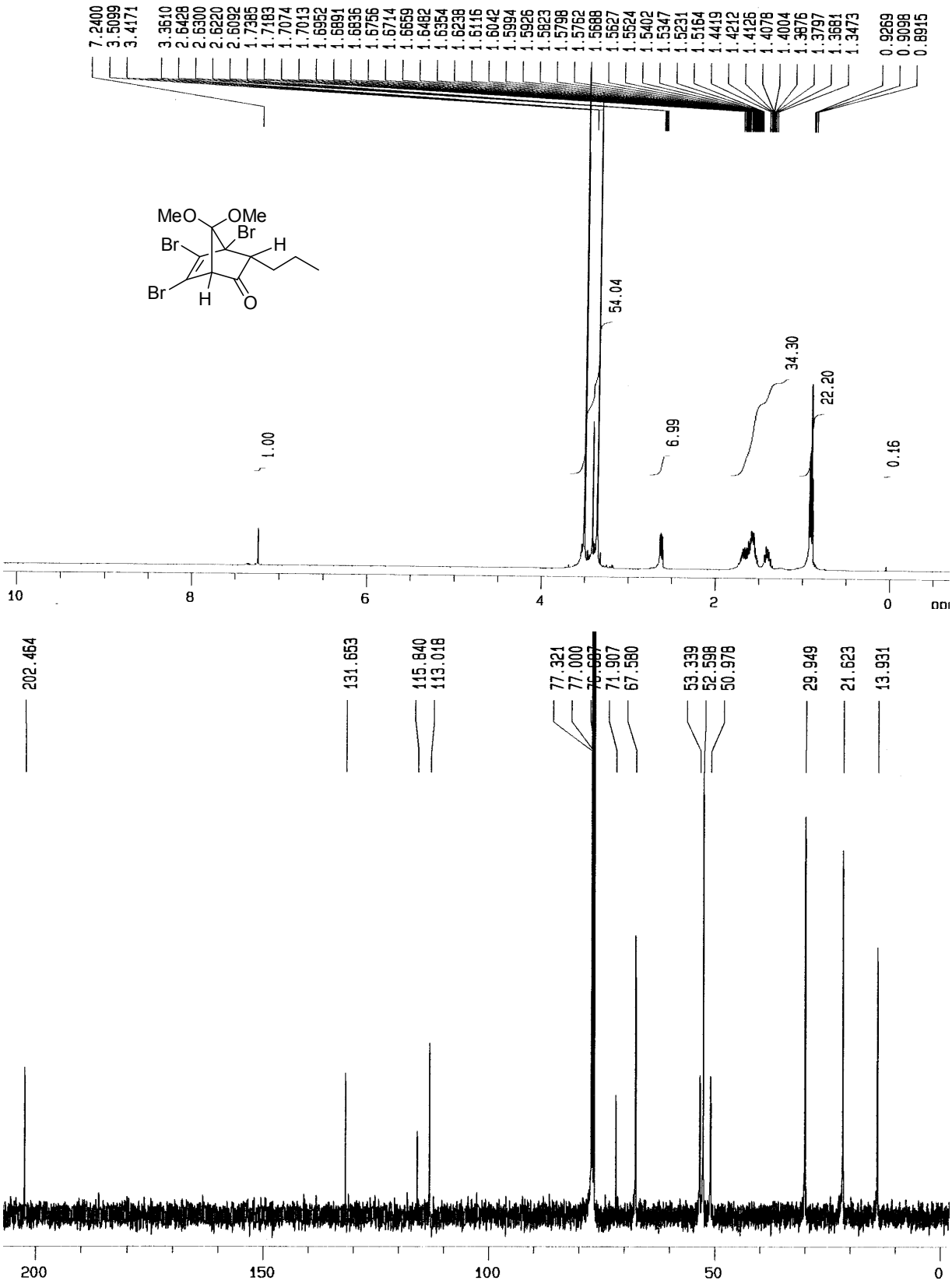

^{1}H NMR (400 MHz) and ^{13}C NMR (100 MHz) of **9b**

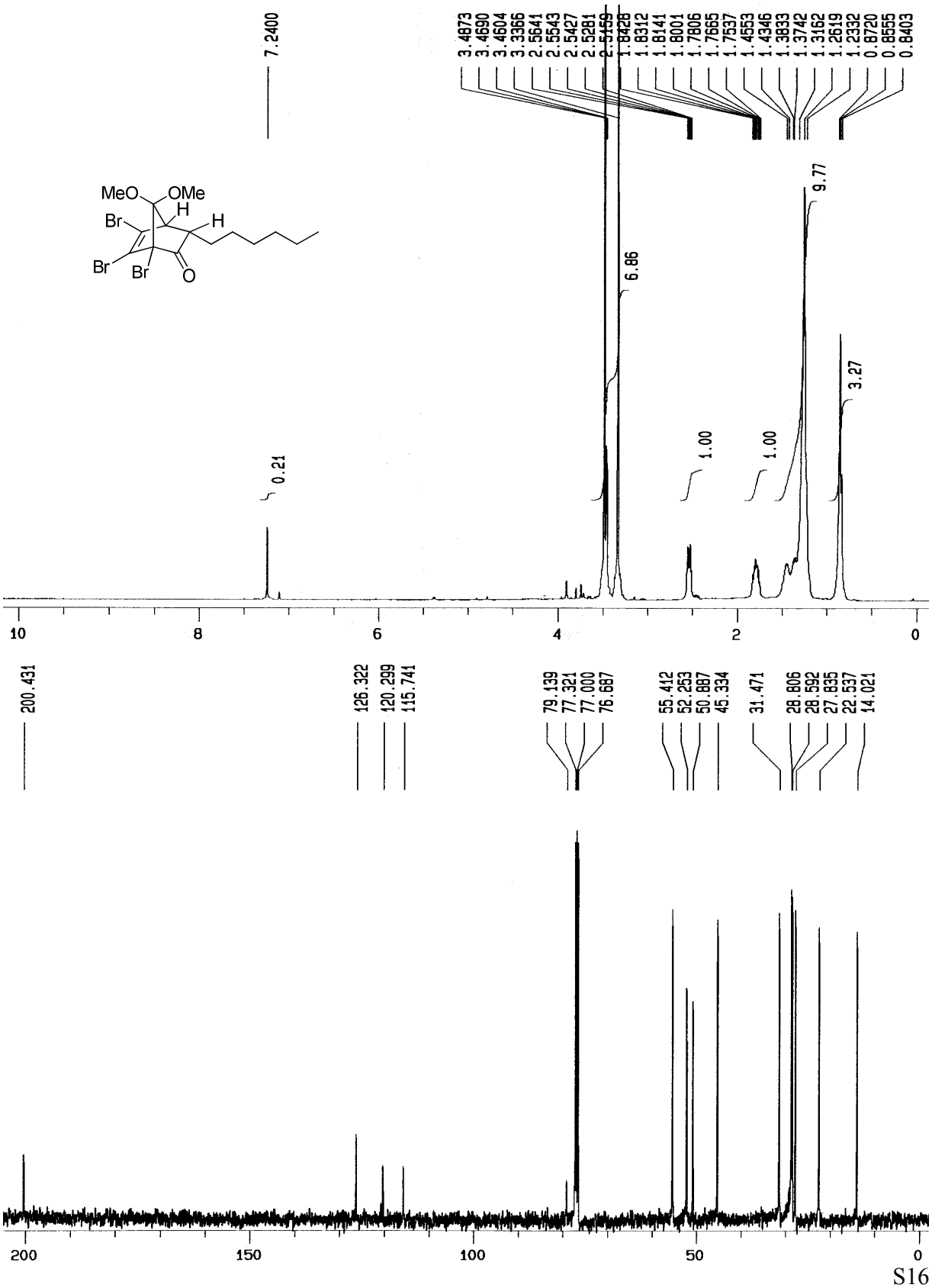

^{1}H NMR (400 MHz) and ^{13}C NMR (100 MHz) of **10b**

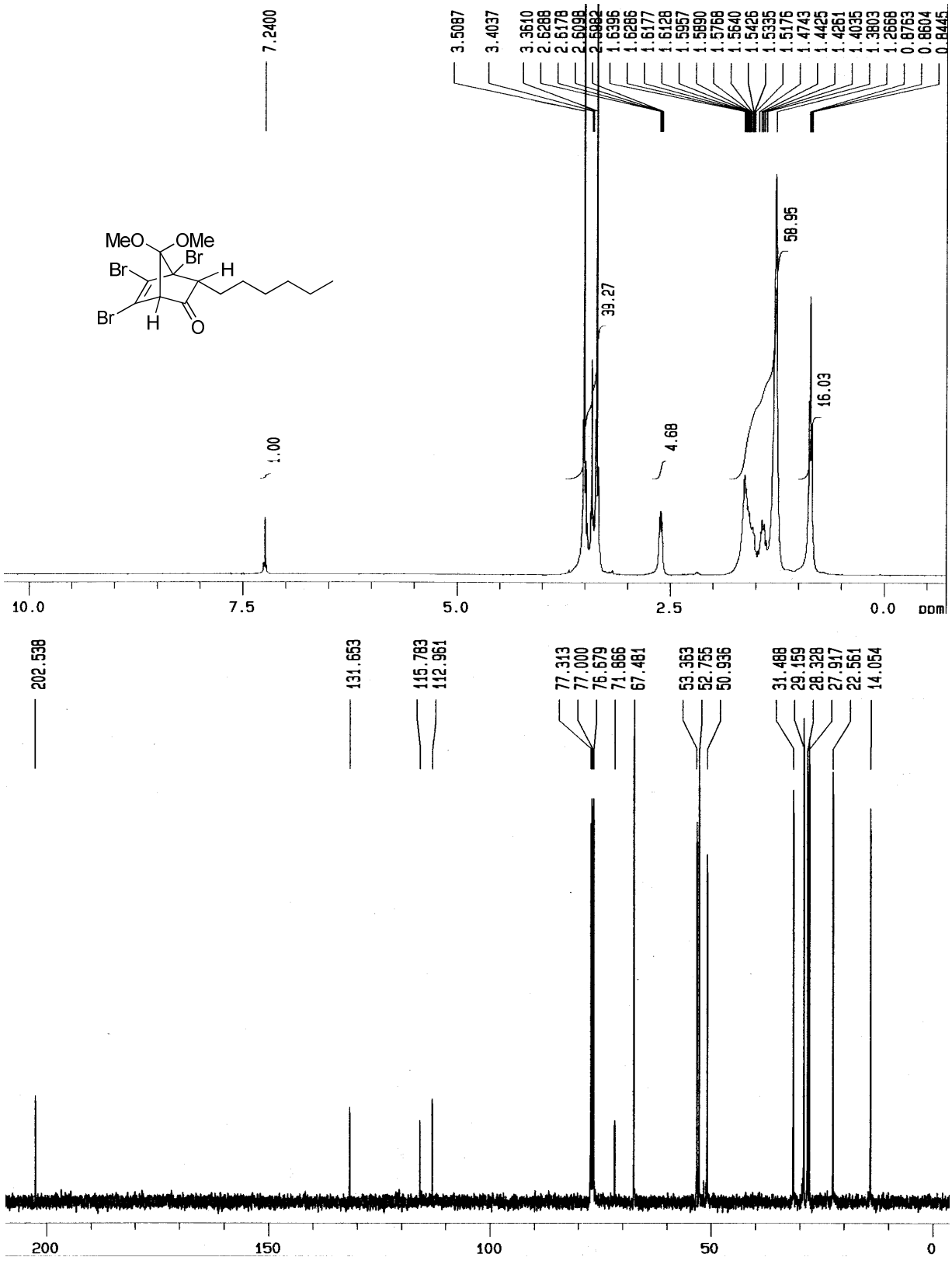

^{1}H NMR (400 MHz) and ^{13}C NMR (125 MHz) of **9c** (partially decomposed to **17c**)

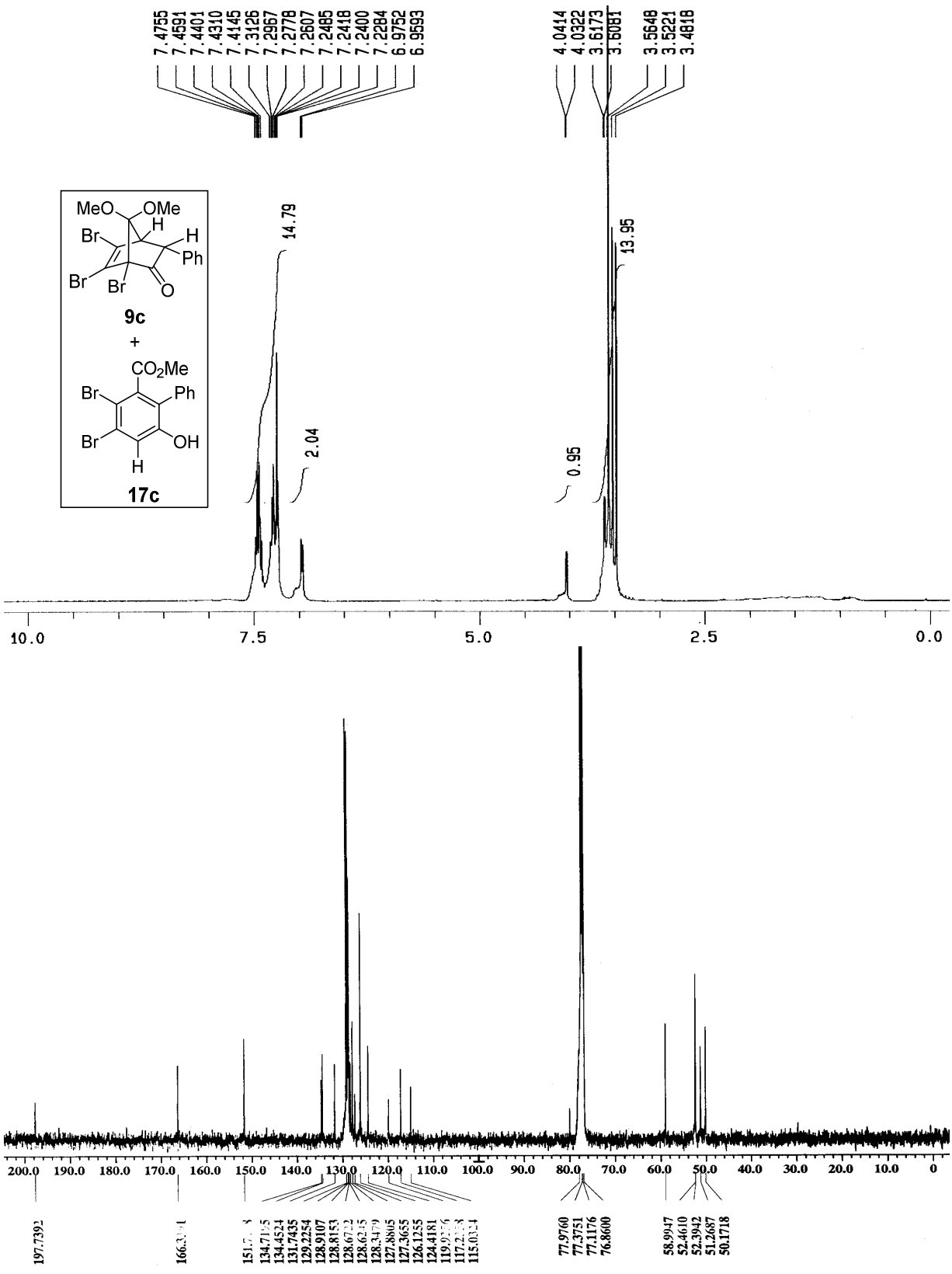

^{1}H NMR (400 MHz) and ^{13}C NMR (125 MHz) of **10c**

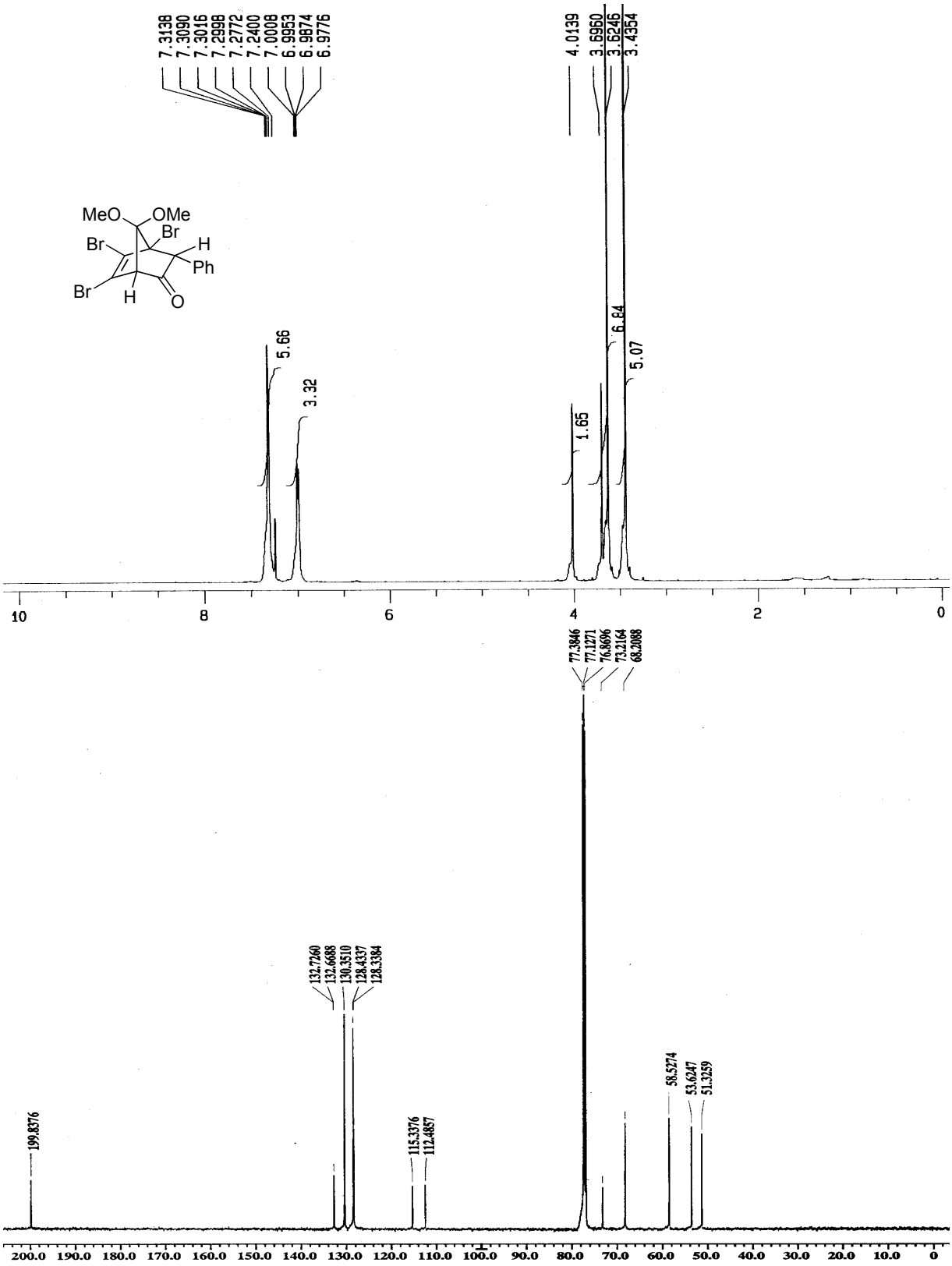

^{1}H NMR (400 MHz) of **9d**

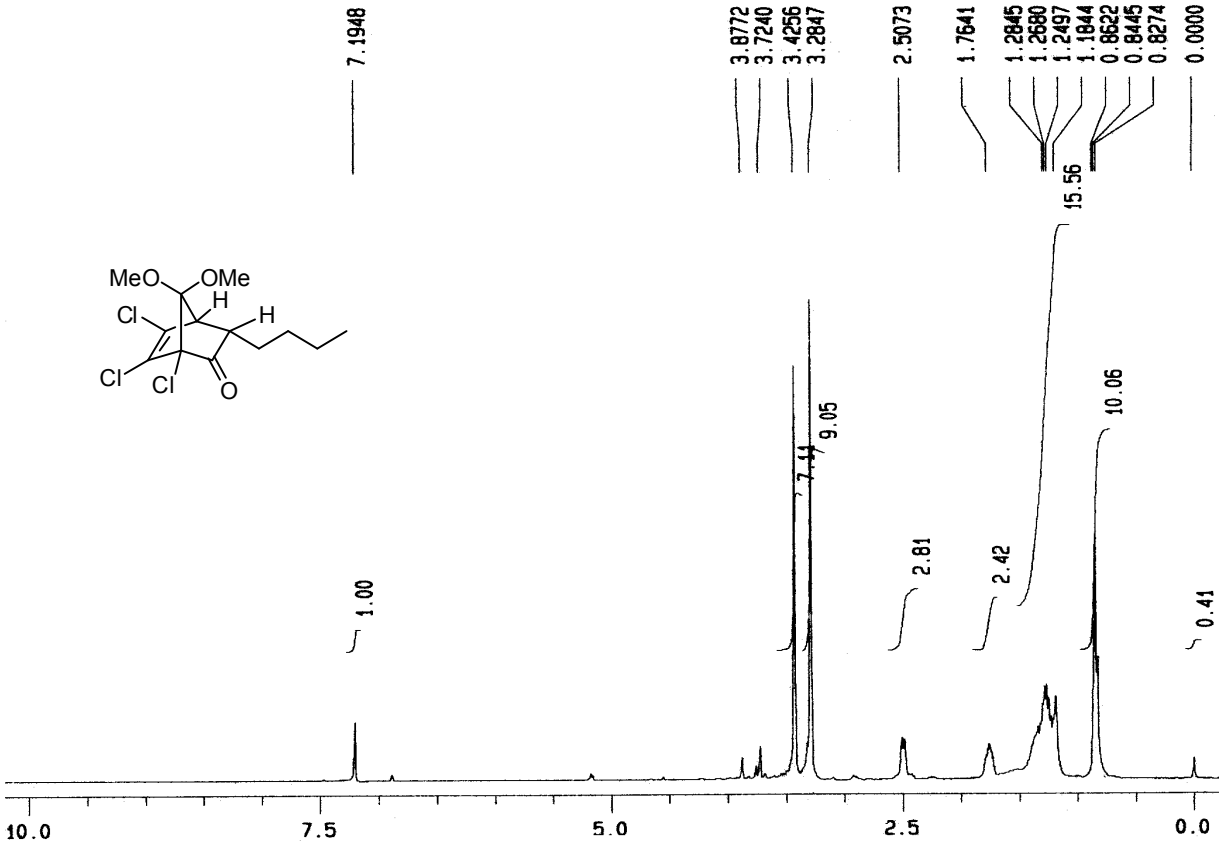

^{1}H NMR (400 MHz) and ^{13}C NMR (100 MHz) of **10d**

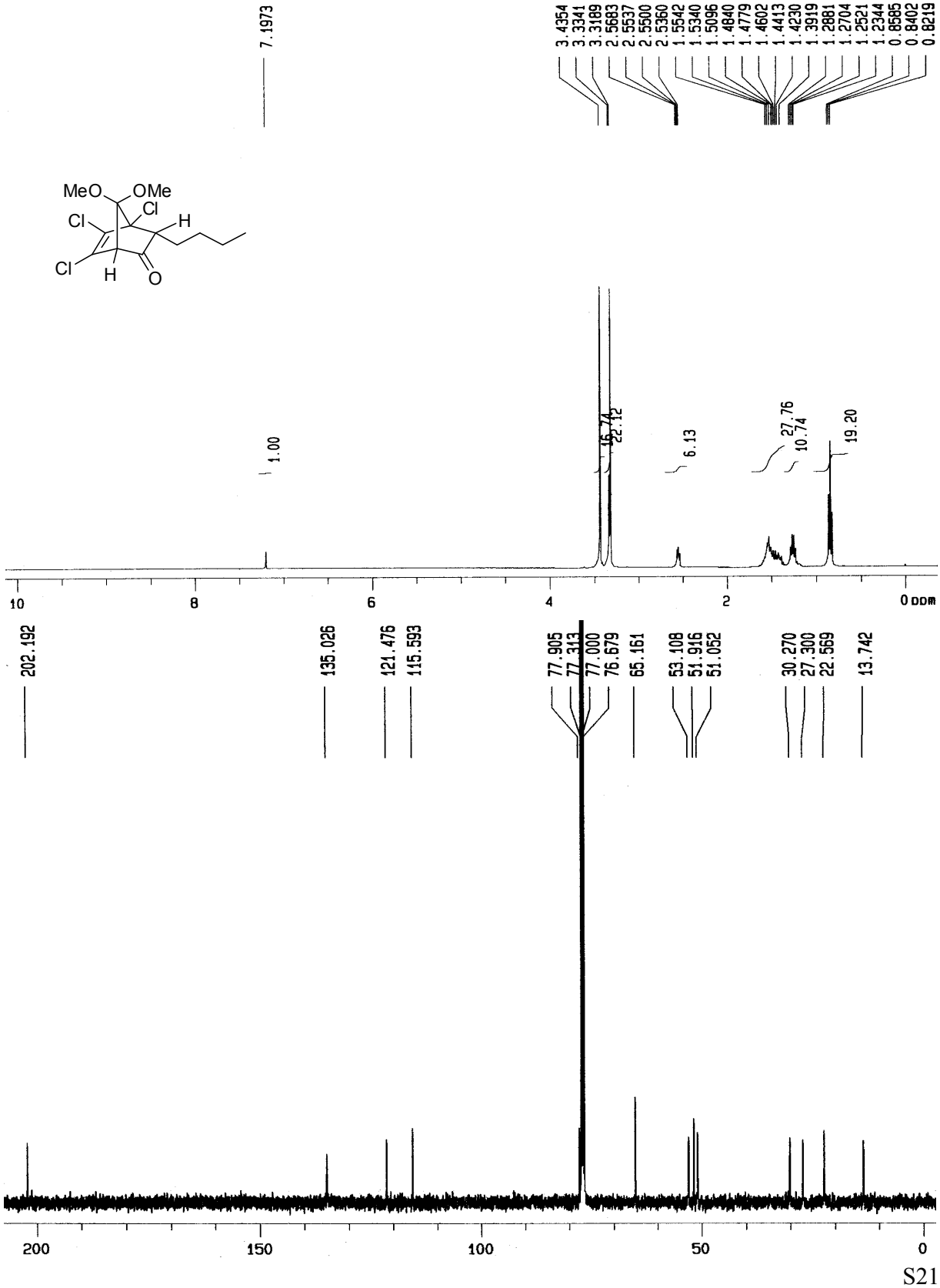

^{1}H NMR (400 MHz) and ^{13}C NMR (100 MHz) of **17a** (obtained from **9a**)

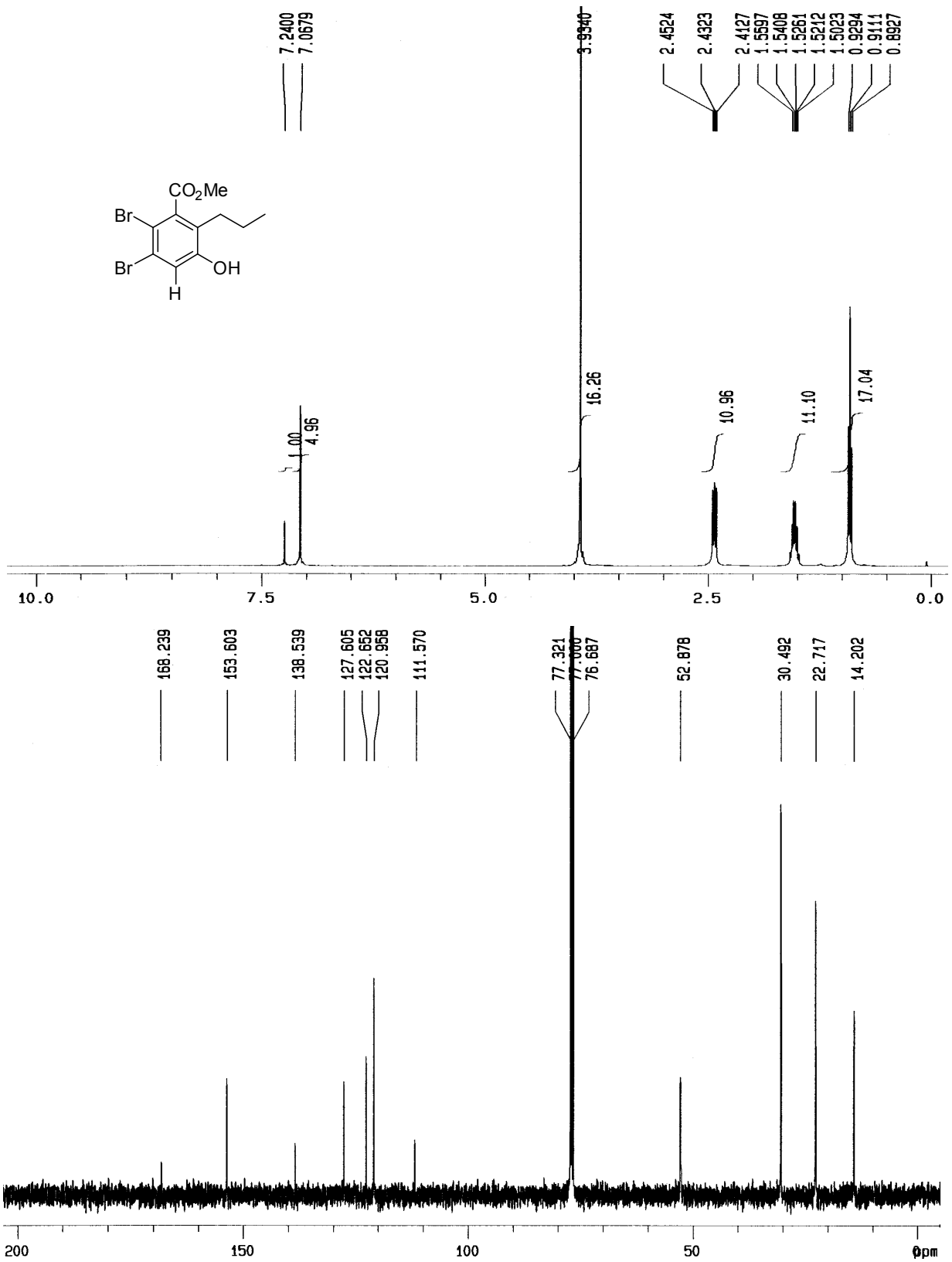

^{1}H NMR (400 MHz) and ^{13}C NMR (125 MHz) of **17a** (obtained from **10a**)

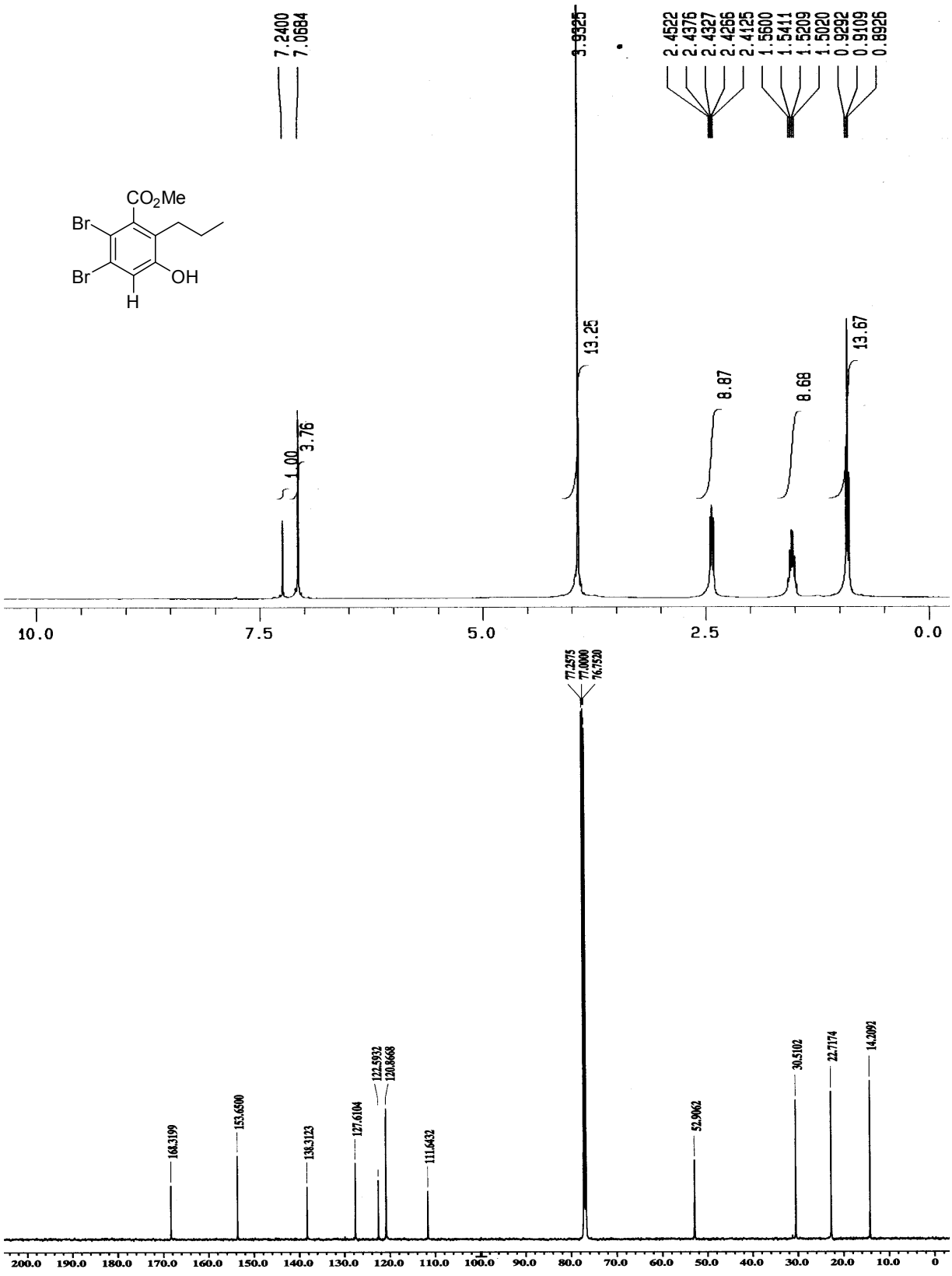

^{1}H NMR (400 MHz) and ^{13}C NMR (100 MHz) of **17b** (obtained from **9b**)

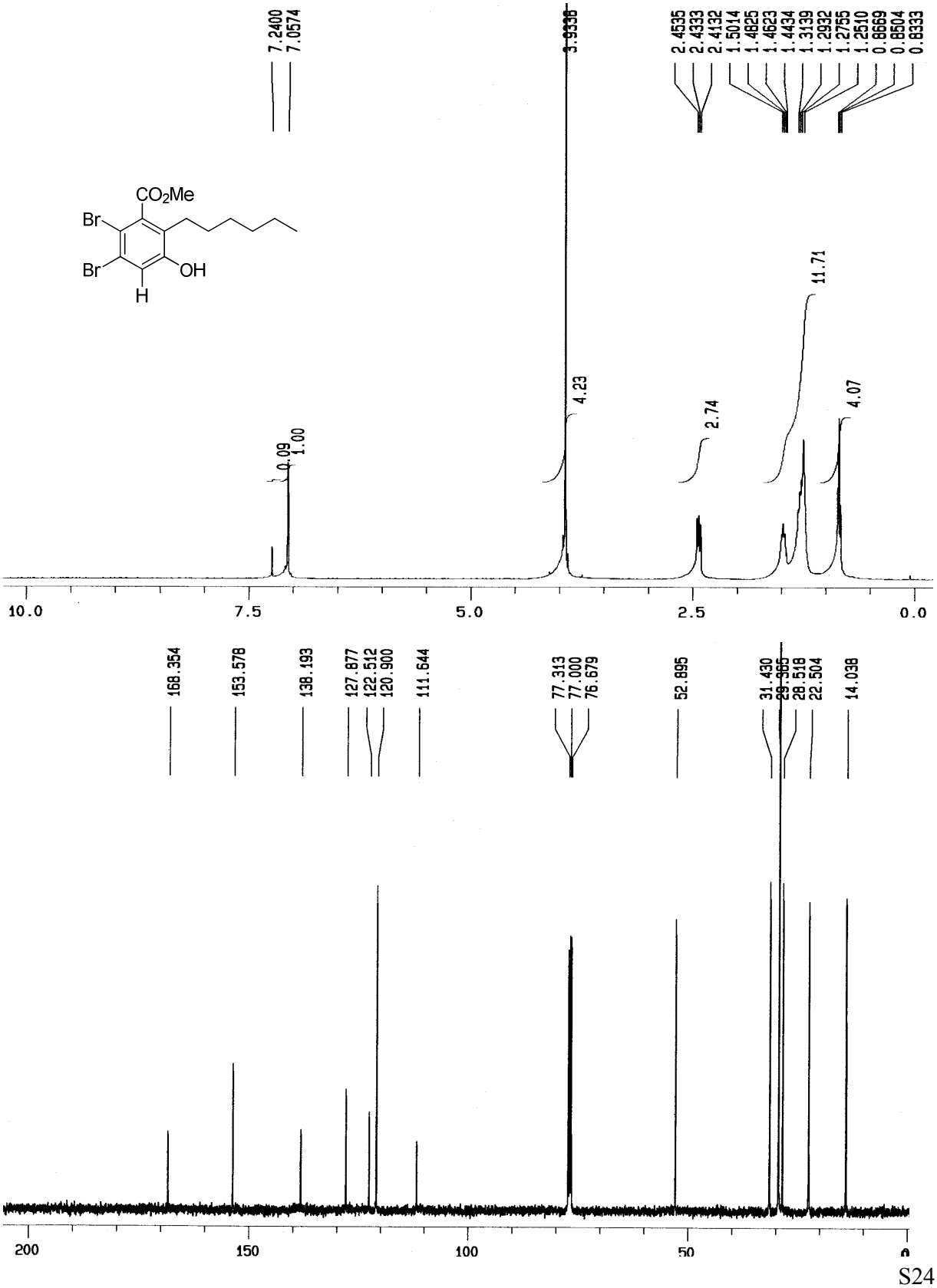

^{1}H NMR (400 MHz) and ^{13}C NMR (100 MHz) of **17b** (obtained from **10b**)

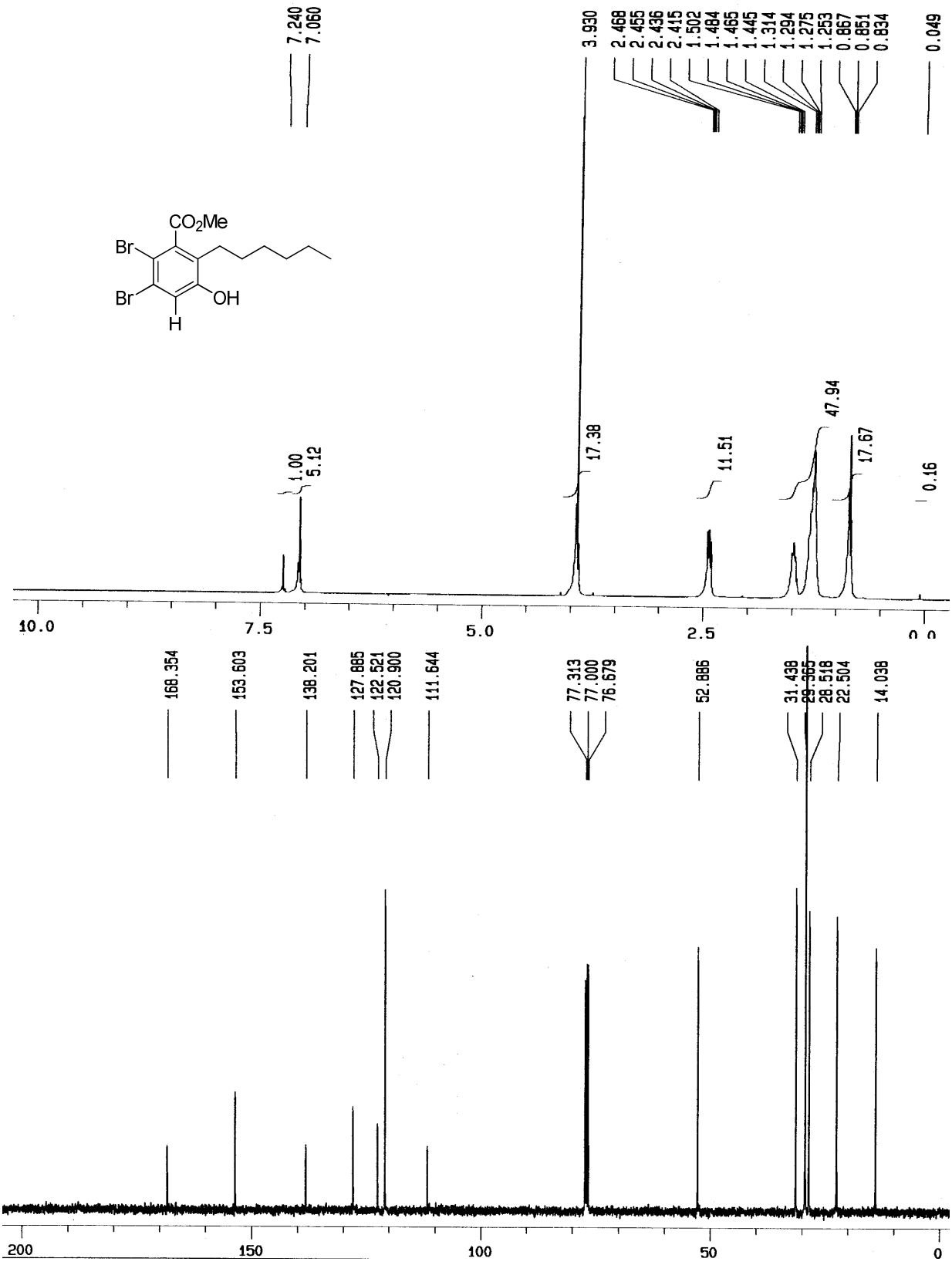

^{1}H NMR (400 MHz) of **17c** (obtained from **9c**)

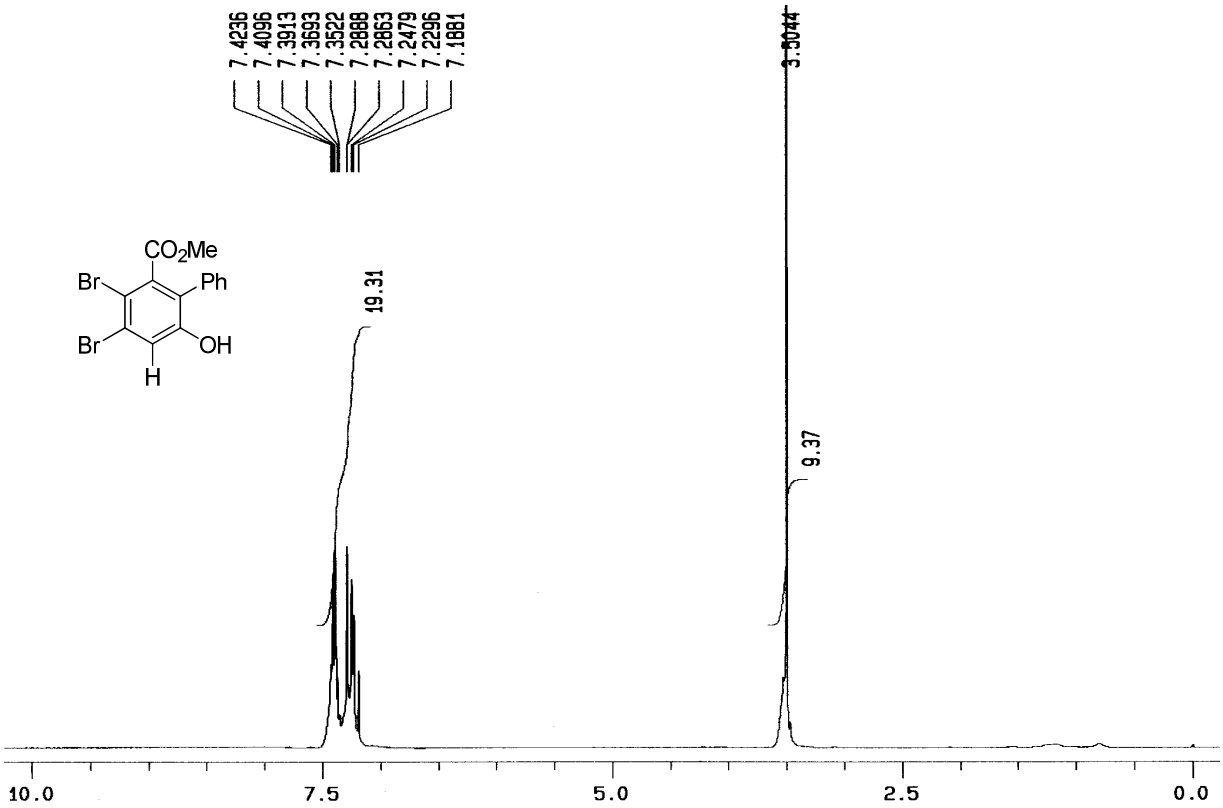

^{1}H NMR (400 MHz) and ^{13}C NMR (125 MHz) of **17c** (obtained from **10c**)

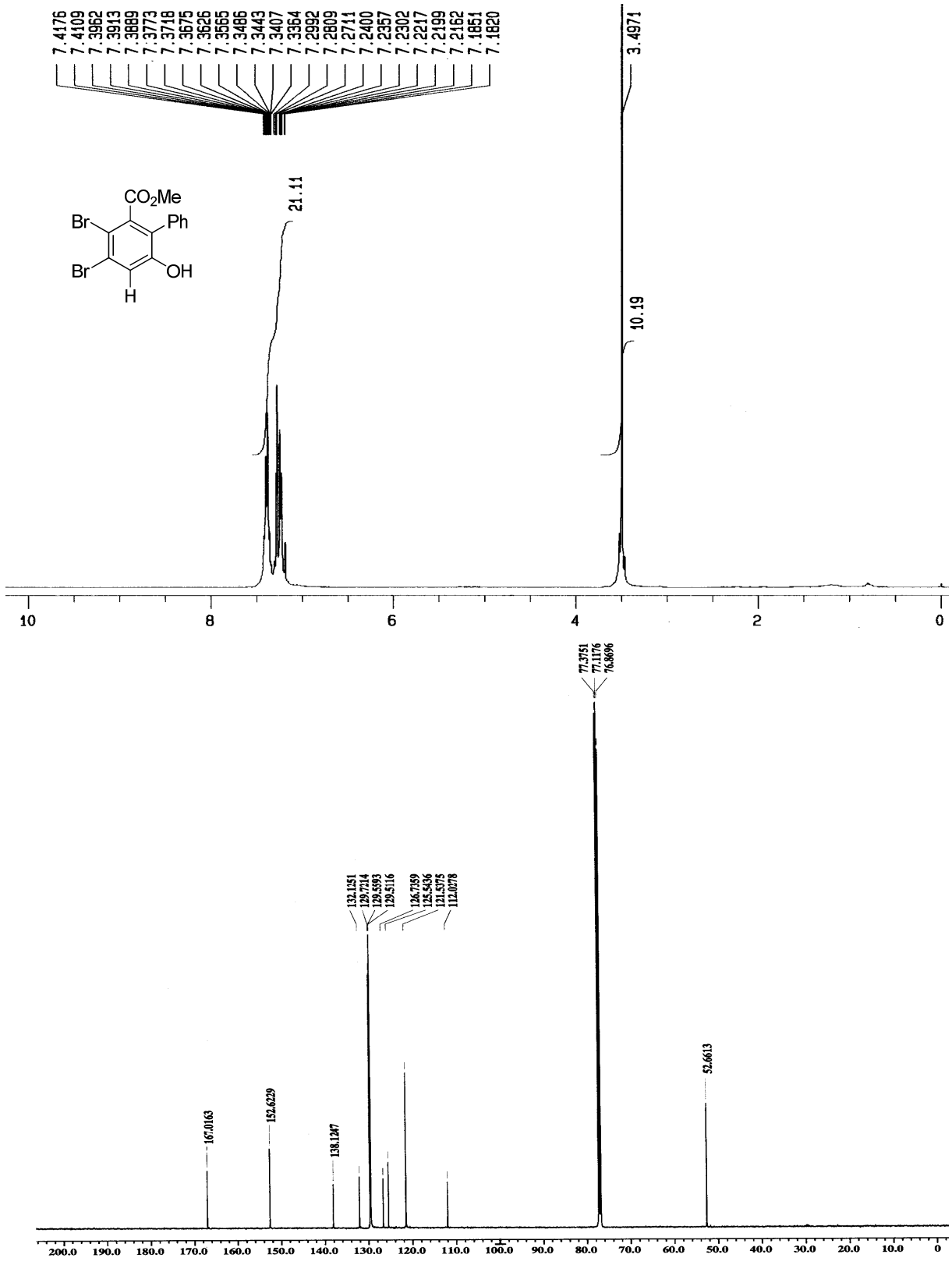

^{1}H NMR (500 MHz) and ^{13}C NMR (125 MHz) of **17d** (obtained from **9d**)

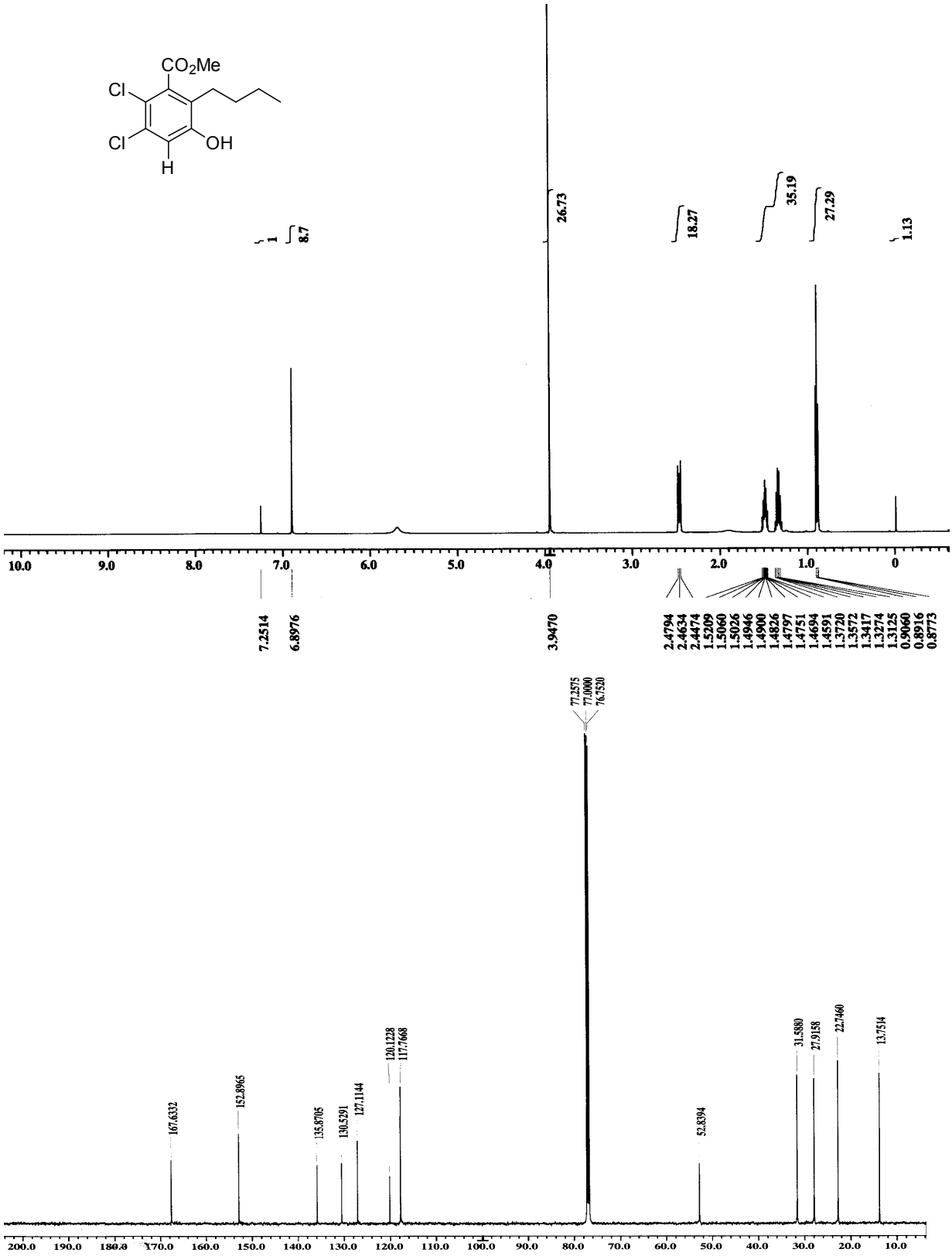

^{1}H NMR (400 MHz) and ^{13}C NMR (125 MHz) of **22-23**

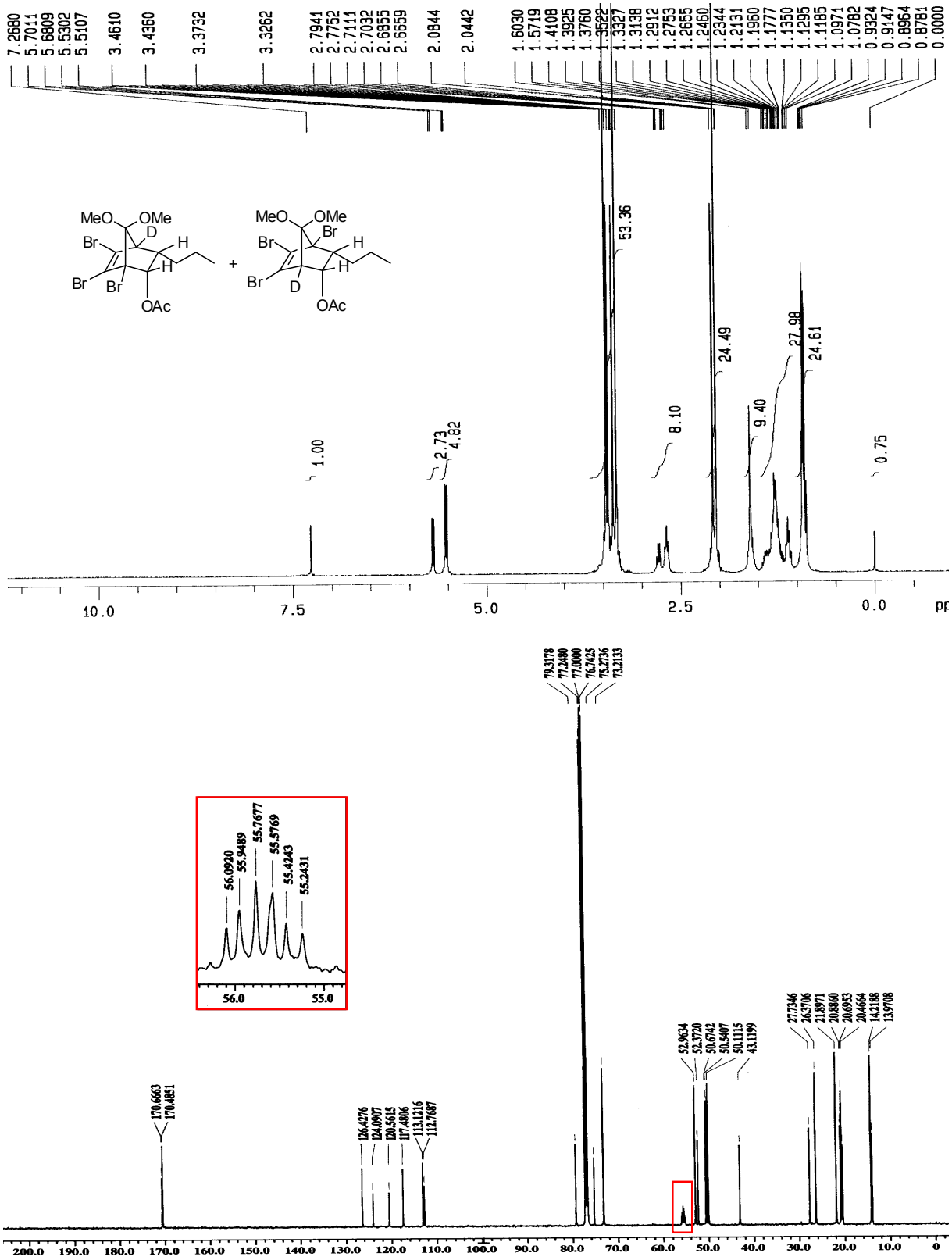

^{1}H NMR (400 MHz) and ^{13}C NMR (125 MHz) of **24**

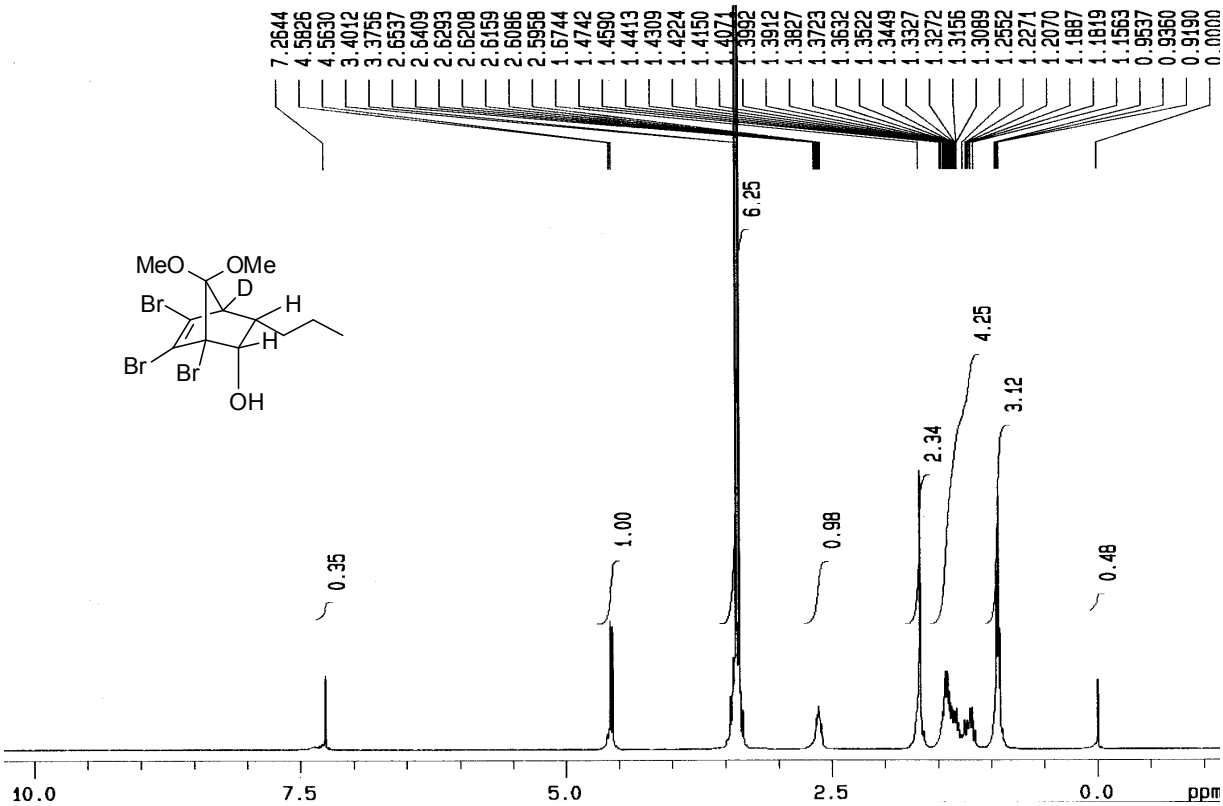

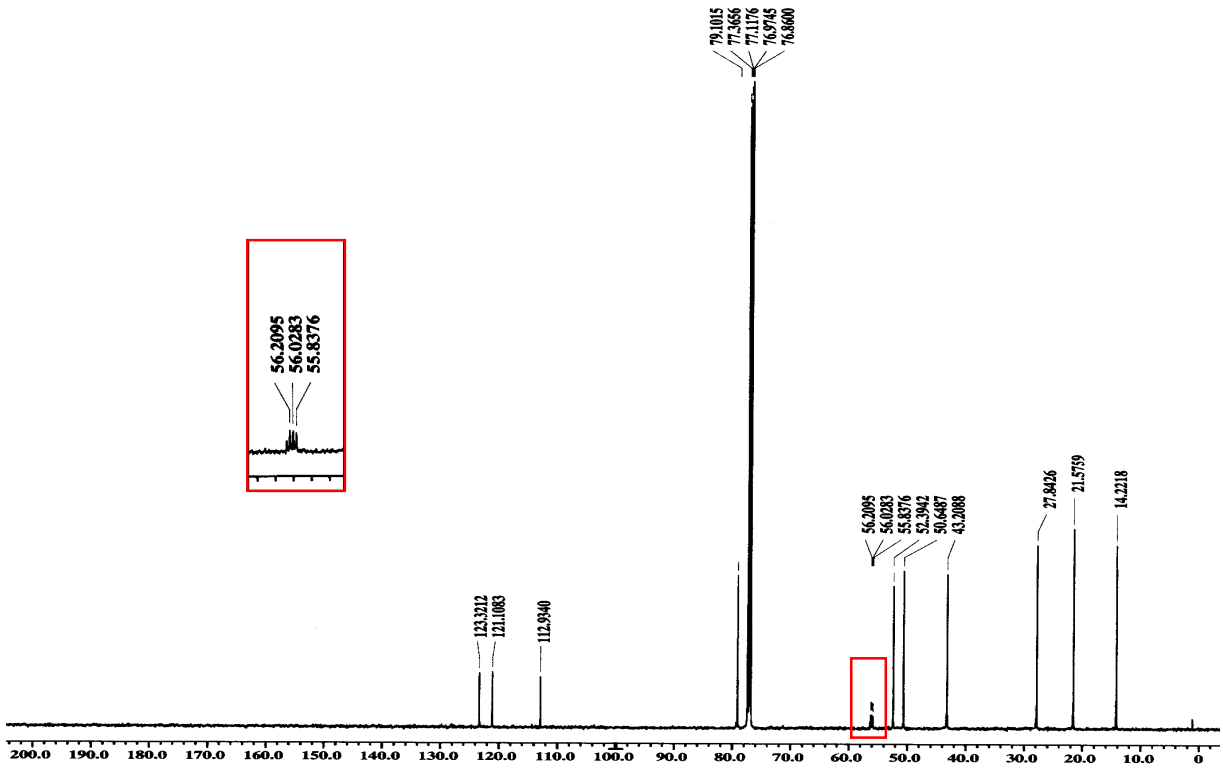

^{1}H NMR (400 MHz) and ^{13}C NMR (125 MHz) of **25**

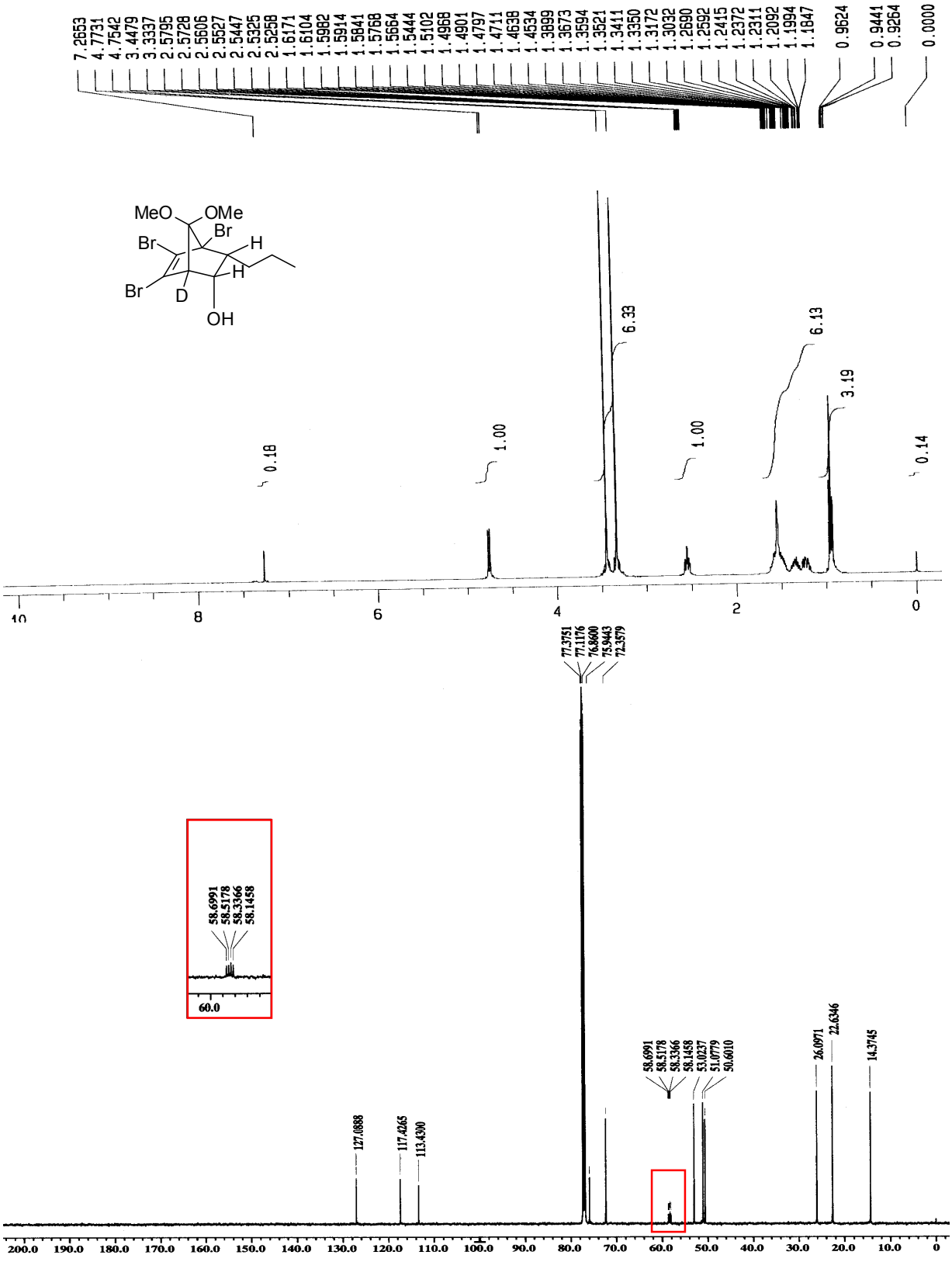

^{1}H NMR (400 MHz) and ^{13}C NMR (125 MHz) of **19**

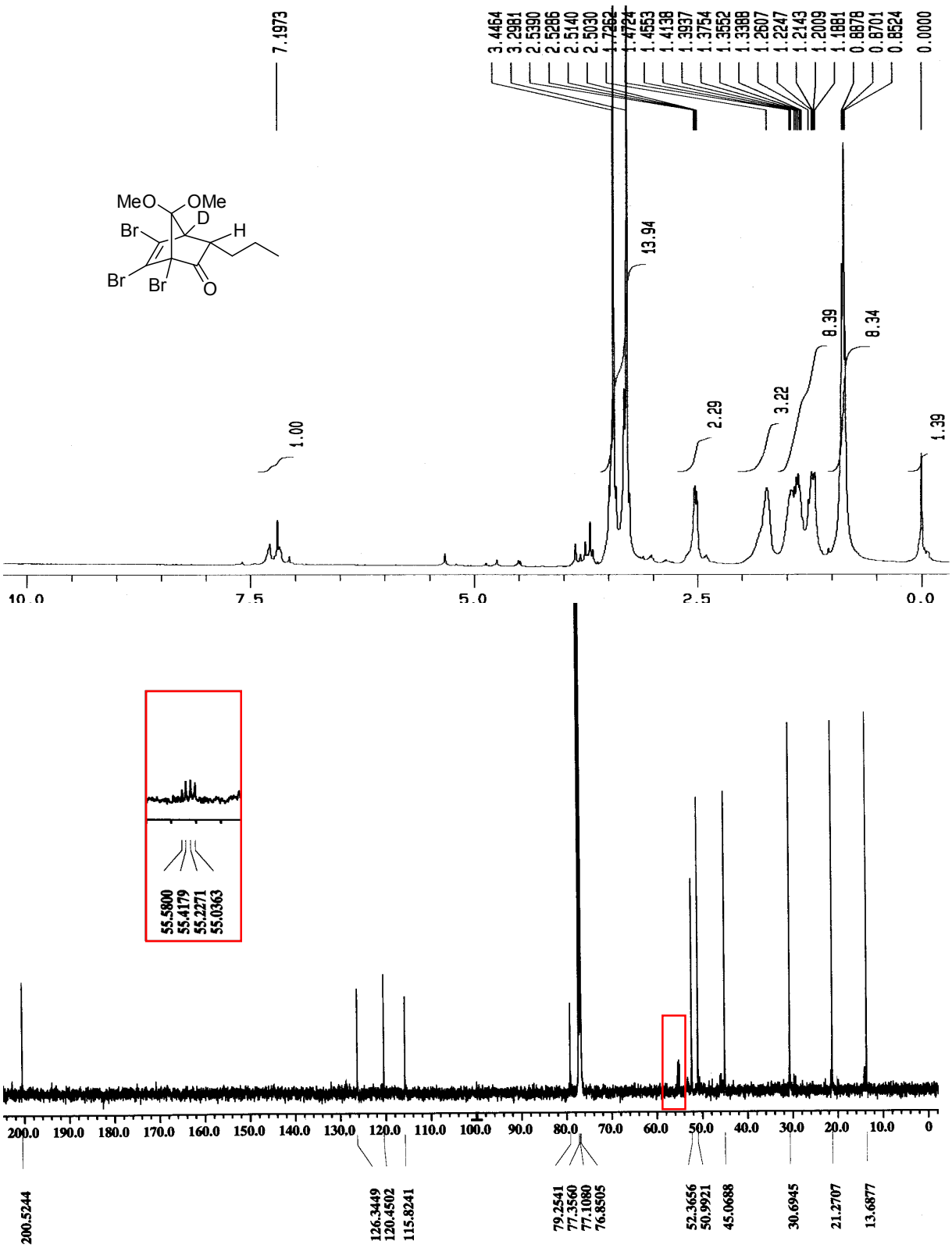

^{1}H NMR (400 MHz) and ^{13}C NMR (125 MHz) of **20**

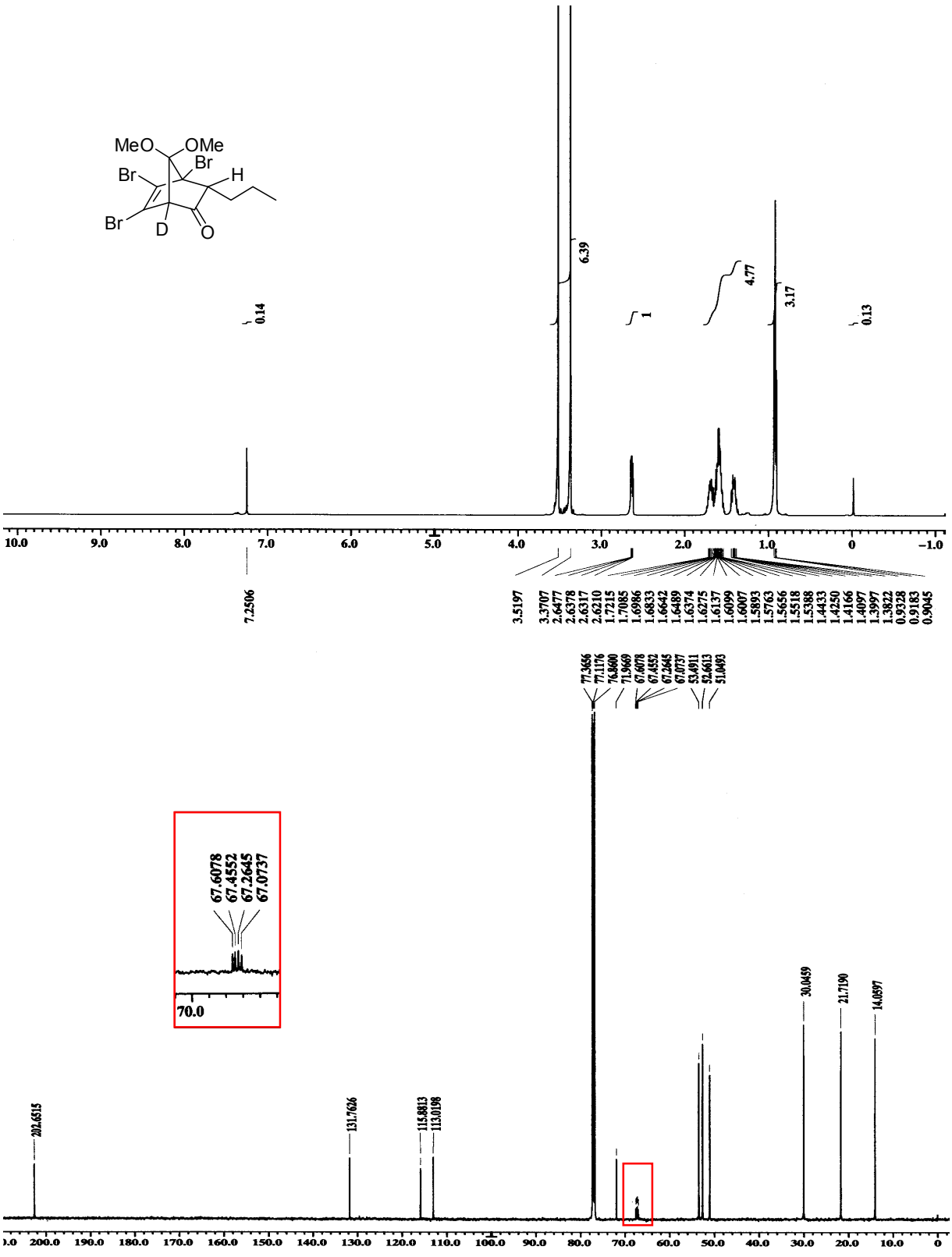

^{1}H NMR (400 MHz) and ^{13}C NMR (125 MHz) of **26** (obtained from **19,** Scheme 4)

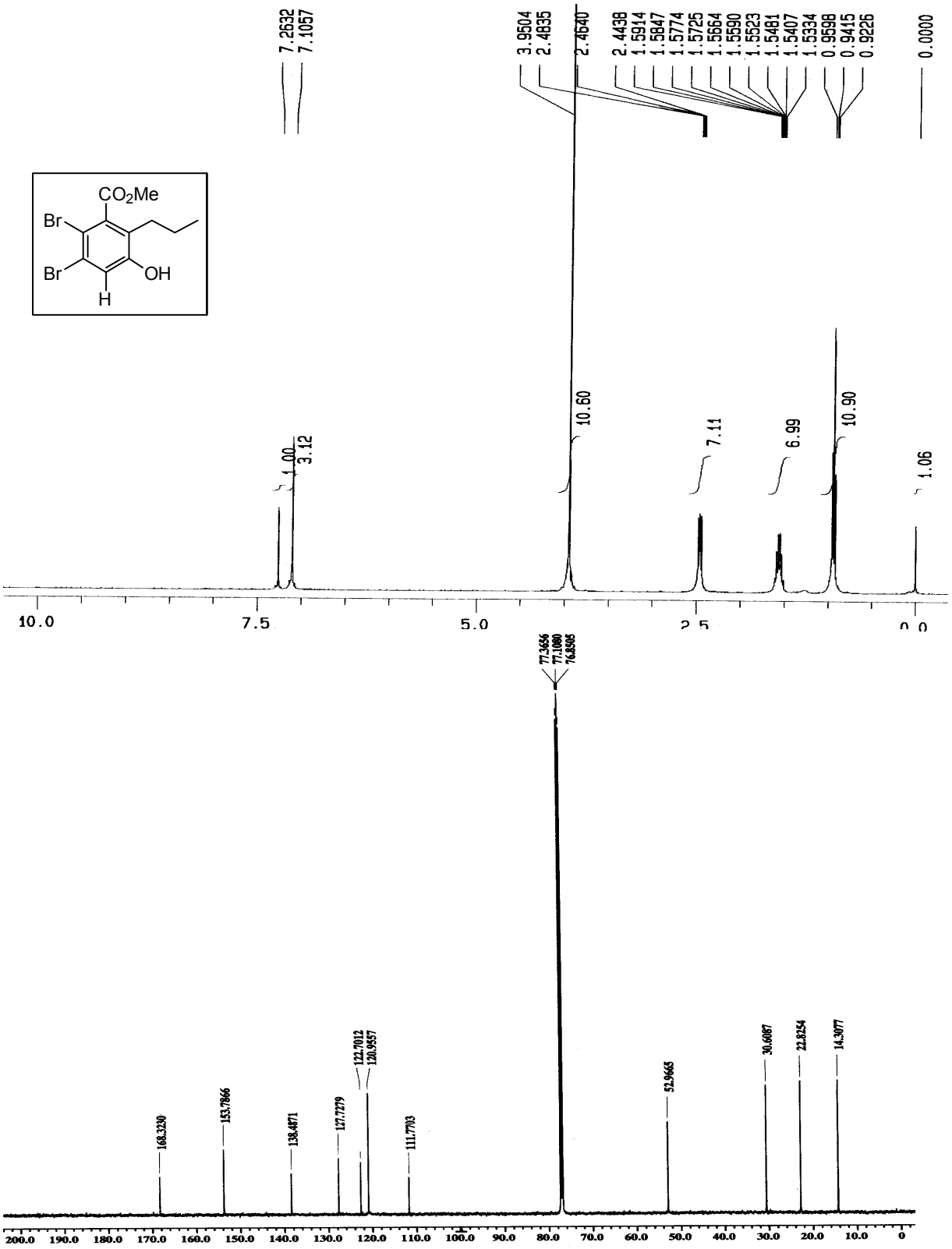

^{1}H NMR (400 MHz) and ^{13}C NMR (125 MHz) of **27** (obtained from **20,** Scheme 4)

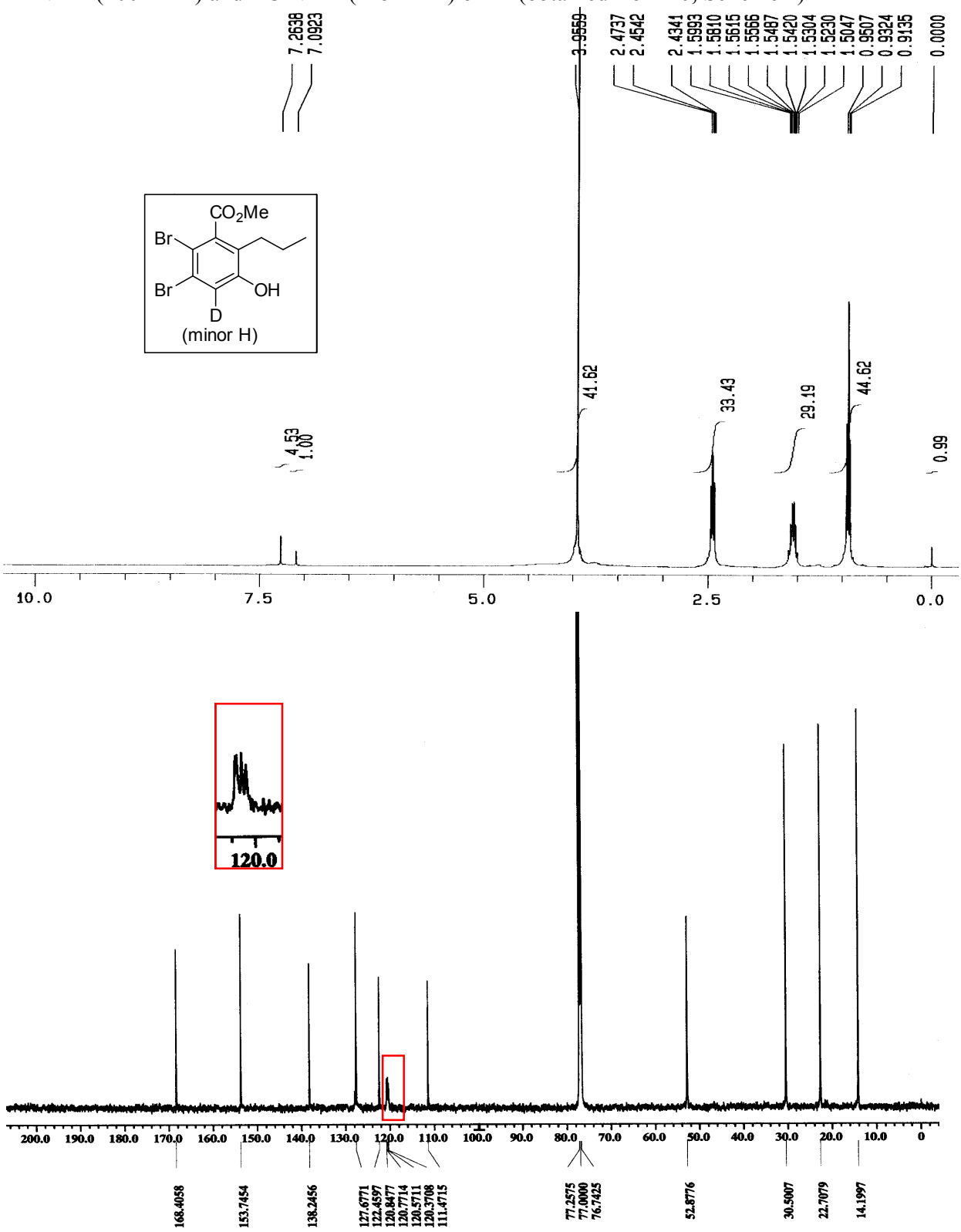

2. Comparison of ^{1}H and ^{13}C NMR spectra of 17a, 26 and 27

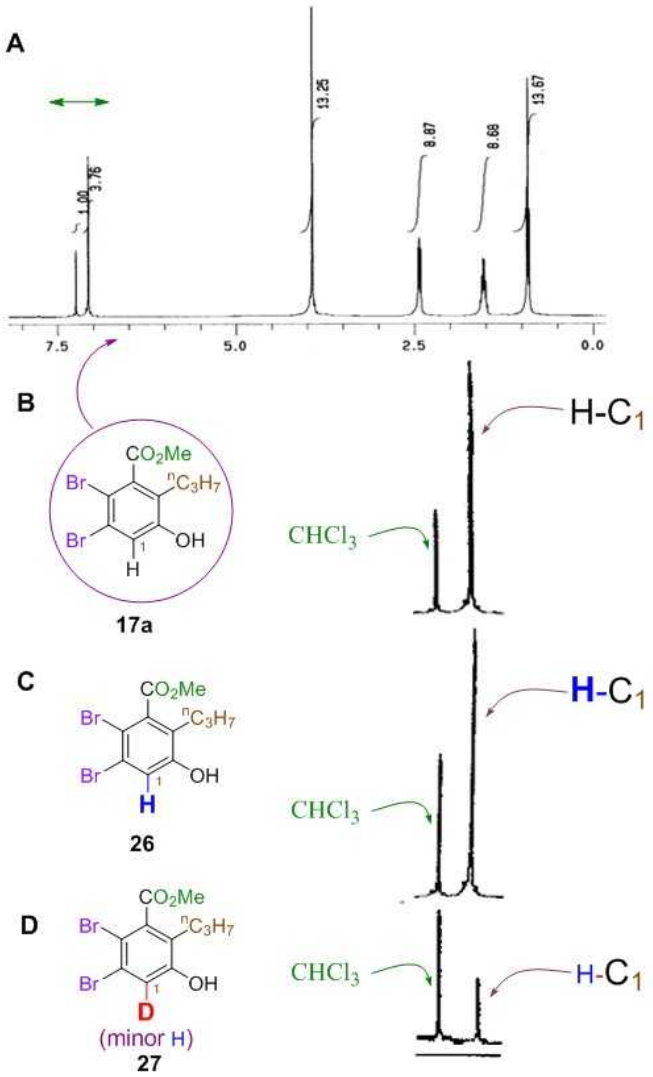

Fig. S1 *Assessment of deuterium incorporation through comparison of ^{1}H NMR spectra of **17a**, **26** and **27**. Fig. S1A : ^{1}H NMR spectra of **17a** in $CDCl_3$; for clarity only selected aromatic regions of **17a**, **26** and **27** are shown in Fig. S1B, S1C and S1D respectively (Residual proton peak of $CDCl_3$ are shown in green).*

As shown in Fig. S1A, the ^{1}H NMR spectrum of **17a** in $CDCl_3$ exhibits one singlet at $\delta = 7.07$ ppm for the aromatic proton at C-1. The phenol derivatives **26** and **27** display altogether similar type of spectra as **17a** excepting the aromatic region due to difference in proton extent at C-1, the expanded portion of which are shown in Fig. S1B-D. Although comparable signal intensity for aromatic protons at C-1 for both **17a** and **26** is observed in the spectra shown in Fig. S1B (of **17a**) and Fig. S1C (of **26**) because of the presence of proton at C-1, a distinct inconsistency can

be visualized with the spectrum in Fig. S1D (of **27**) containing a peak in the aromatic region, whose intensity is substantially decreased, owing to predominant deuterium presence at C-1.

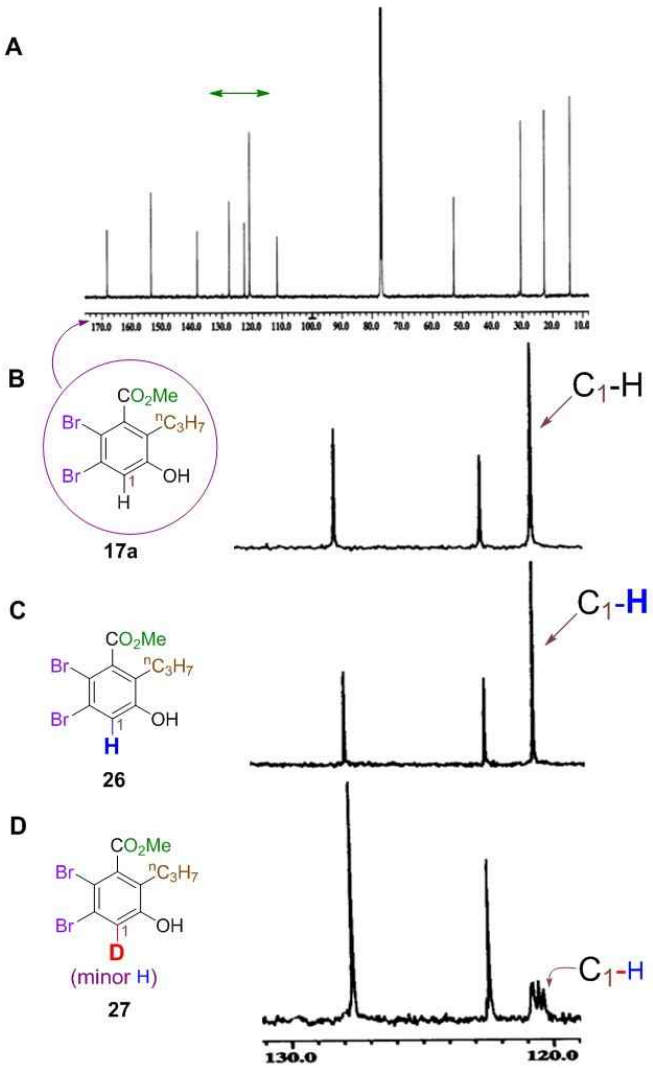

Fig. S2 *Assessment of deuterium incorporation through comparison of ^{13}C NMR spectra of **17a**, **26** and **27**. Fig. S2A: ^{13}C NMR spectra of **17a** in $CDCl_3$; for clarity only selected aromatic regions of **17a**, **26** and **27** are shown in Fig. S2B, S2C and S2D respectively.*

On the other hand, as shown in Fig. S2A, the ^{13}C NMR spectrum of **17a** in $CDCl_3$ exhibits an intense peak at δ = 120.9 ppm due to aromatic carbon C-1. The phenol derivatives **26** and **27** display analogous spectra to that of **17a** but showing deviations in the aromatic region, the expanded portion of which are compared in Fig. S2B-D. While the spectra in Fig. S2B (of **17a**) and Fig. S2C (of **26**) remain almost same owing to the presence of proton at C-1 but a

distinguishable difference can be detected with that in Fig. S2D (of **27**) wherein the aforesaid strong peak due to aromatic carbon C-1 attached to hydrogen has been replaced with a less intense peak of multiplet nature on account of major deuterium occurrence.

3. Plausible mechanism for fragmentation of mono-deuteriated norbpornyl ketones 19 and 20.

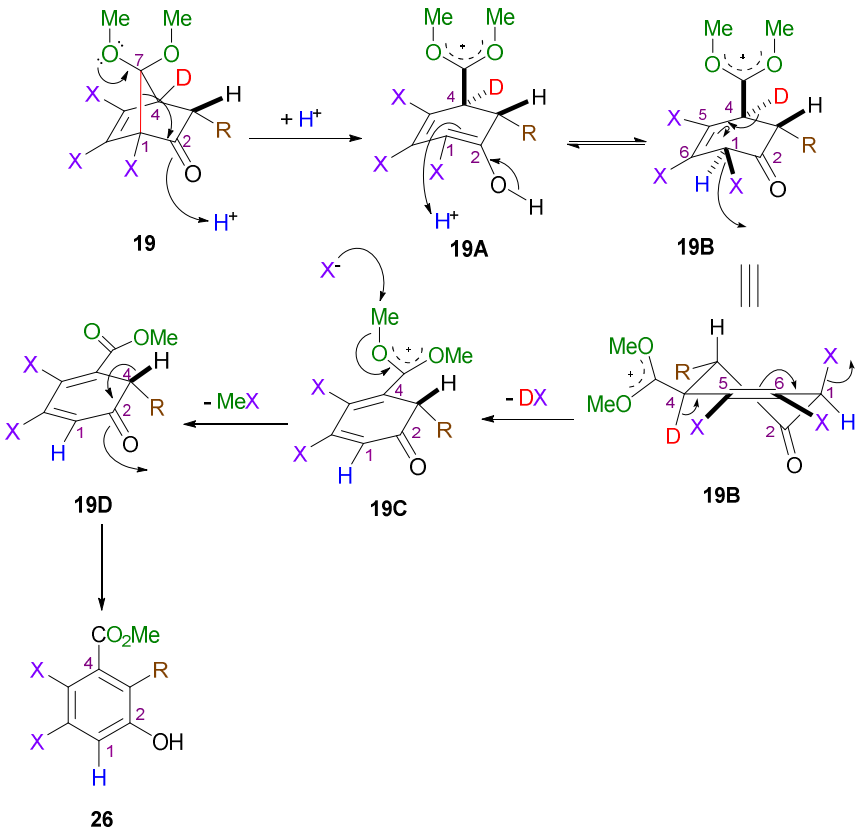

Fig. S3 *Plausible mechanism for fragmentation of mono-deuteriated norbpornyl ketone* ***19****.*

Acid catalyzed fragmentation of **19**, possessing 4-D and 1-X, furnishes oxocarbenium ion **19A** which undergoes protonation at the C1-C2 double bond to generate **19B**. At this stage, the acidic deuterium atom 4-D and halogen 1-X are positioned pseudo-axially and thus undergo a facile 1,4-elimination to form **19C**. Hence the final product **26** obtained from **19C** in the usual way remains devoid of any observable deuterium presence (Fig. S3).

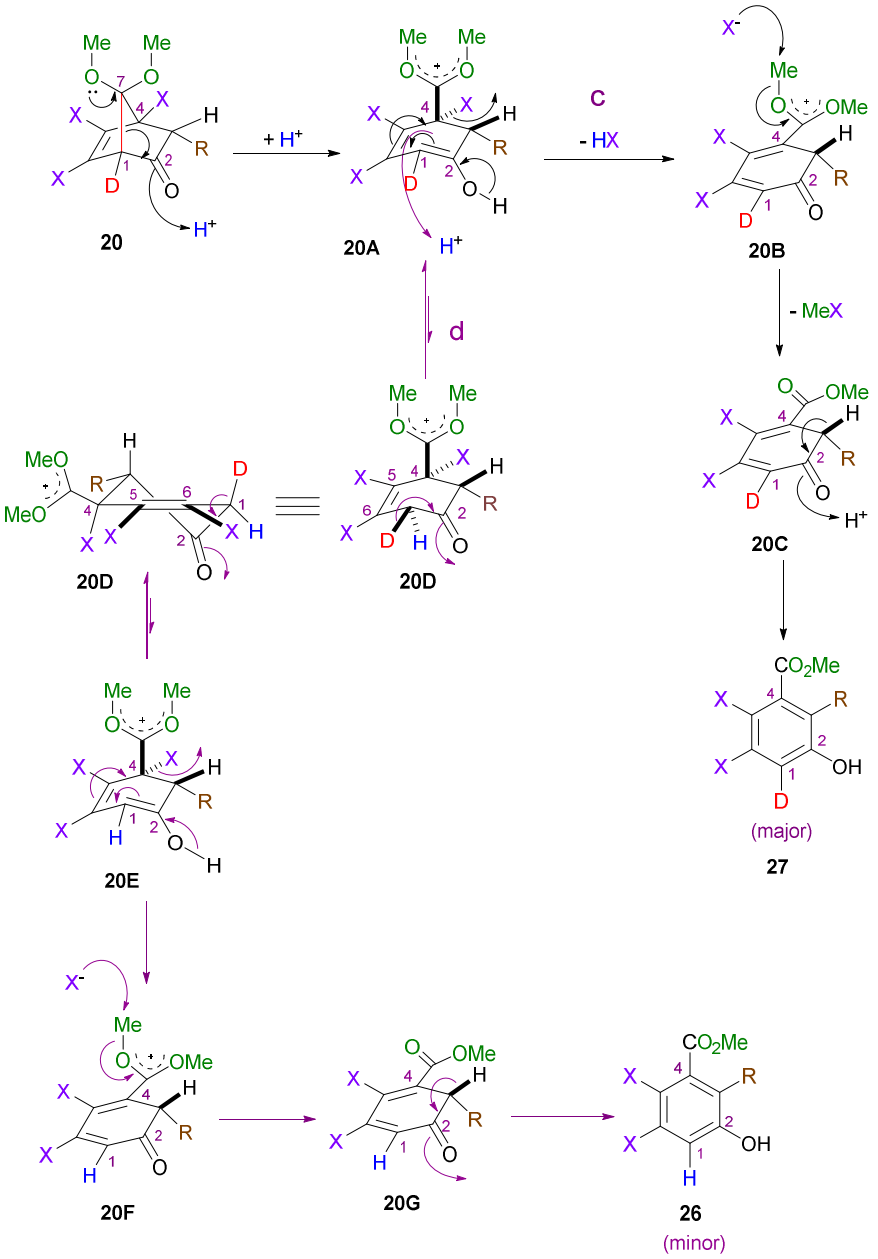

Fig. S4 *Plausible mechanism for fragmentation of mono-deuteriated norbpornyl ketone* ***20****.*

On the other hand, acid-mediated cleavage of **20**, bearing 1-D and 4-X, generates intermediate oxocarbenium ion **20A** which eventually ends up in the formation of phenol derivative **27** in the usual fashion without requiring the involvement of 1-D in the entire mechanism (route **c**, Fig. S4). Thus the final product **27** is characterized by predominant deuterium presence at the aromatic carbon C-1. However, rationalization of minor amount of proton occurrence at C-1 of **27** demands additional pathways to be invoked (route **d**, Fig. S4). It can be postulated that some

of **20A** before transforming to **20B** can also undergo protonation at the β carbon of dienol functionality (i.e. C-1) present in **20A** from the less hindered face thereby forcing the existing deuterium atom 1-D to the more hindered face generating **20D**. Thus during enolisation, preferential involvement of pseudo-axially oriented deuterium atom 1-D of **20D** can be presumed giving rise to **20E** where C-1 position remains occupied by proton and not by deuterium. So the final product obtained from it *via* usual route would definitely consist of proton at C-1 of the aromatic skeleton of **27** thereby constituting the rationale for minor product formation.

4. Overall acid-catalyzed fragmentation of tetra-,[1] tri- (present results) and di-[2] halo norbornyl ketones.

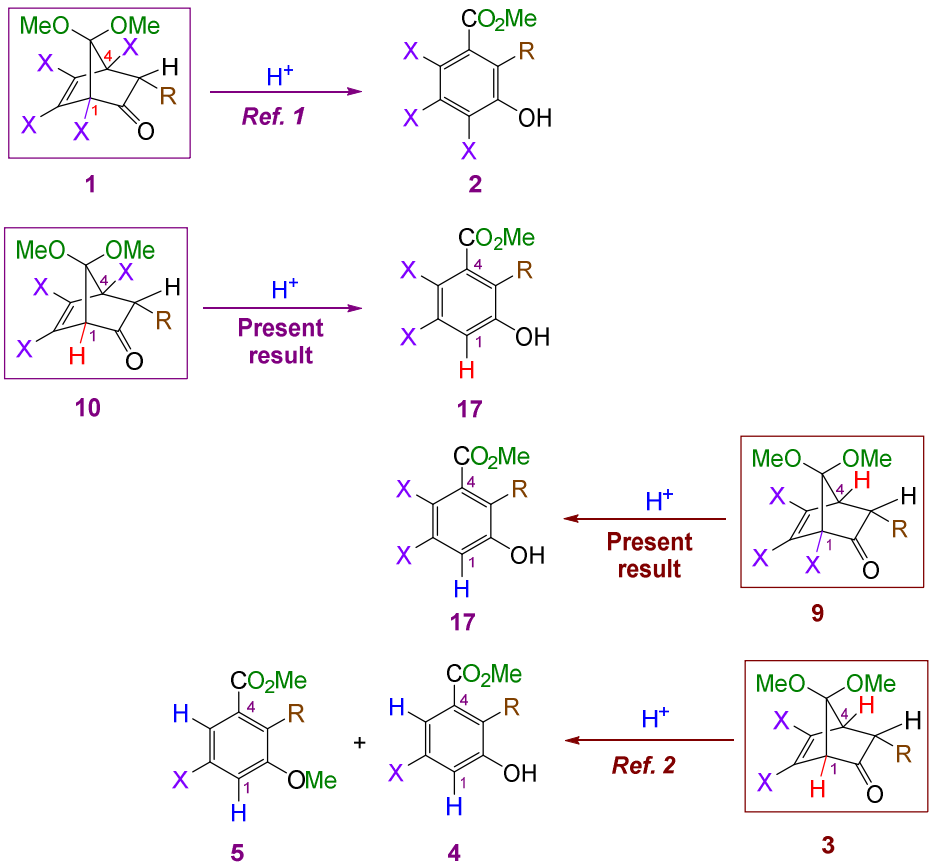

Fig S5*. Pictorial representation of acid-catalyzed fragmentation of tetra-,[1] tri- (present results) and di-[2] halo norbornyl ketones.*

It represents two pairs of bicyclic ketones **1** & **10** and **3** & **9** where each one of a pair differs from the other one at the substitution pattern at C-1 bridgehead position while the other

bridgehead substitution (i.e. at **C-4**) remains same. The obvious conclusion coming out from the above representation is that starting from $C_mH_nX_o$ system (**1/3/9/10**) we eventually end up with $C_{m-1}H_{n-3}X_{o-1}$ system (**2/4/17/17**) indicating overall loss of MeX. When the bridgehead position C-4 is occupied by halogen (as C-4-X in **1** and **10**), then irrespective of the nature of the substituent in the other bridgehead position C-1, major amount of products are formed through similar mechanistic pathways without necessitating the involvement of the C-1 substituent thereby retaining the C-1 substituent in the final products **17**. On the other hand, when the C-4 substituent is hydrogen (as 4-H in **9** and **3**), then the reaction pathway is dictated by the nature of the substituent at other bridgehead position C-1; if it is *hydrogen* (i.e. 1-H as in **3**) then product formation takes place *via* exclusive protonation at δ carbon (i.e. **C-5**) of dienol moiety formed *in situ*, while β carbon (i.e. **C-1**) would undergo similar protonation if *halogen* remains at C-**1** (i.e. 1-X as in **9**). From these observation, we can conclude that bridgehead substituents are responsible in steering the reaction pathways to be followed and among the two substituents, one occupying position away from the carbonyl group (i.e. C-**4**) has the precedence over the other located vicinal to carbonyl moiety (i.e. C-**1**).

5. X-ray crystal data for 17c

Single crystal X-ray data for **17c** were collected at 100 K on a Bruker SMART APEX-II CCD diffractometer using graphite-monochromated MoKα radiation (λ = 0.71069 Å). The linear absorption coefficients, scattering factors for the atoms, and the anomalous dispersion corrections were taken from International Tables for X-ray Crystallography. Data integration and reduction were processed with SAINT[3a] software. An empirical absorption correction was applied to the collected reflections with SADABS[3b] using XPREP[3c]. The structure was solved by the direct method using SHELXTL[3d] and was refined on *F*2 by full-matrix least-squares technique using the SHELXL-97[3e] program package. The lattice parameters and structural data are tabulated in Table S1.

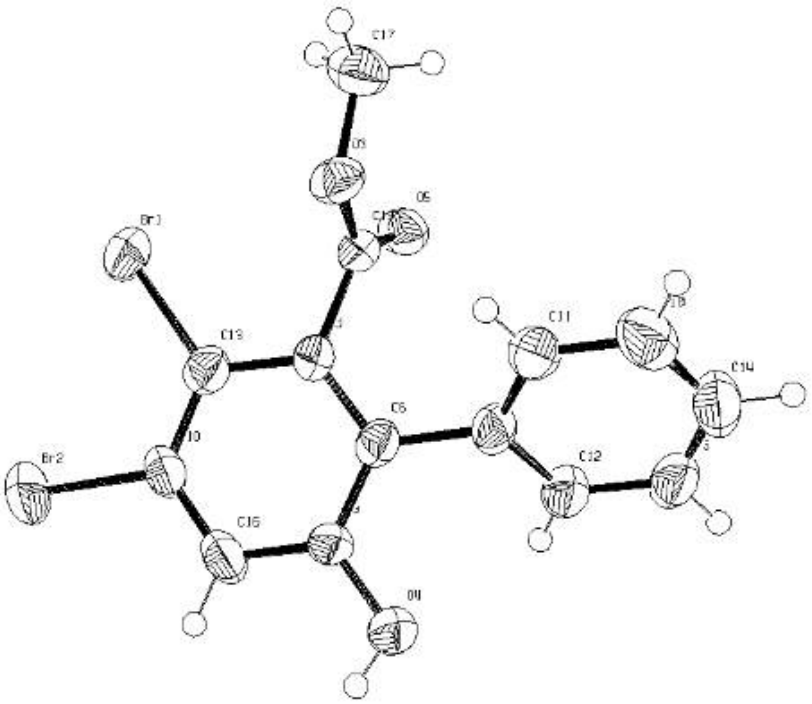

Fig. S6 *ORTEP structure of compound* ***17c****. (50% thermal ellipsoid probability)*

Table S1 Crystallographic information for **17c**

CCDC no	1404444
Empirical formula	C_{14} H_{10} Br_2 O_3
Formula weight	386.04
Color of crystal	Colourless
Temperature	100(1) K
Radiation	MoK_α
Wavelength	0.71069 Å
Crystal system	Orthorhombic
Space group	*P*n21a
a, Å	7.871(5) Å
b, Å	11.094(5) Å
c, Å	15.506(5) Å
V, $Å^3$	1354.0(11) $Å^3$
Z	4
ρ_{calc} Mg/m^3	1.894
μ, mm^{-1}	5.987
F(000)	752
Independent refl.	2782
Reflns. used (I>2σ(I))	1865
R_{int} value	0.0527
Refinement method	Full-matrix least-squares on F^2
GOOF (Goodness-of-fit)	1.045
R indices [I>2σ(I)]	R_1= 0.0471, wR_2= 0.1135
R indices (all data)	R1=0.0828 wR2=0.1563

6. References

1 (a) F. A. Khan and S. Choudhury, *Eur. J. Org. Chem.*, 2006, 672–676; (b) F. A. Khan and S. Choudhury, *Synth. Commun.*, 2006, **36**, 3749–3760.

2 F. A. Khan and S. Choudhury, *Eur. J. Org. Chem.*, 2010, 2954–2970.

3 (a) SAINT+, version 6.02; Bruker AXS: Madison, WI, 1999; (b) G. M. Sheldrick, SADABS,

Empirical Absorption Correction Program; University of Göttingen: Göttingen, Germany, 1997; (c) XPREP, 5.1 ed.; Siemens Industrial Automation Inc.: Madison, WI, 1995; (d) G. M. Sheldric, SHELXTL Reference Manual, version 5.1; Bruker AXS: Madison, WI, 1997; (e) G. M. Sheldric, SHELXL-97, Program for Crystal Structure Refinement; University of Göttingen: Göttingen, Germany, 1997.